

# Robust Localization and Tracking of UAVs in OTFS-based Networks

Alessandro Nordio, *Member, IEEE*, Carla Fabiana Chiasserini, *Fellow, IEEE*, Emanuele Viterbo, *Fellow, IEEE*

**Abstract**—We consider the problem of accurately localizing  $N$  unmanned aerial vehicles (UAV) in 3D space where the UAVs are part of a swarm and communicate with each other through orthogonal time-frequency space (OTFS) modulated signals. Each receiving UAV estimates the multipath wireless channel on each link formed by the line-of-sight (LoS) transmission and by the single reflections from the remaining  $N - 2$  UAVs. The estimated power delay profiles are communicated to an edge server, which is in charge of computing the exact location and speed of the UAVs. To obtain the UAVs locations and velocities, we propose an iterative algorithm, named Turbo Iterative Positioning (TIP), which, using a belief-propagation approach, effectively exploits the time difference of arrival (TDoA) measurements between the LoS and the non-LoS paths. Enabling a full cold start (no prior knowledge), our solution first maps each TDoA's profile element to a specific ID of the reflecting UAV's. The Doppler shifts measured by the OTFS receivers associated with each path are also used to estimate the UAV's velocities.

The localization of the  $N$  UAVs is then derived via gradient descent optimization, with the aid of turbo-like iterations that can progressively correct some of the residual errors in the initial ID mapping operation. Our numerical results, obtained also using real-world traces, show how the multipath links are beneficial to achieving very accurate localization and speed of all UAVs, even with a limited delay-Doppler resolution. Robustness of our scheme is proven by its performance approaching the Cramer-Rao bound.

**Index Terms**—Tracking, Localization, OTFS, UAVs

## I. INTRODUCTION

Accurate localization stands as a crucial element in the repertoire of applications that forthcoming beyond 5G communication networks are anticipated to empower [2]. This encompasses applications such as ensuring safety in vehicular networks and facilitating missions related to area exploration, rescue operations, and relief efforts, all of which can be achieved through swarms of unmanned aerial vehicles (UAVs) [3], [4]. In situations where GPS signals are restricted or absent, the process of localizing these communicating nodes typically involves measuring their distances, which is performed by

Alessandro Nordio is with CNR-IEIIT, Torino, Italy; Carla Fabiana Chiasserini is with Politecnico di Torino, Torino, Italy; Emanuele Viterbo is with Monash University, Melbourne, Australia.

This work was partially supported by the European Union under the Italian National Recovery and Resilience Plan (NRRP) of NextGenerationEU, partnership on "Telecommunications of the Future" (PE00000001 - program "RESTART"), and by the Project: "SoBigData.it - Strengthening the Italian RI for Social Mining and Big Data Analytics". E. Viterbo's work is supported by the Australian Research Council (ARC) through the Discovery project: DP200100096.

A preliminary version of this work was presented at Globecom'23 [1].

This work has been submitted to the IEEE for possible publication. Copyright may be transferred without notice, after which this version may no longer be accessible.

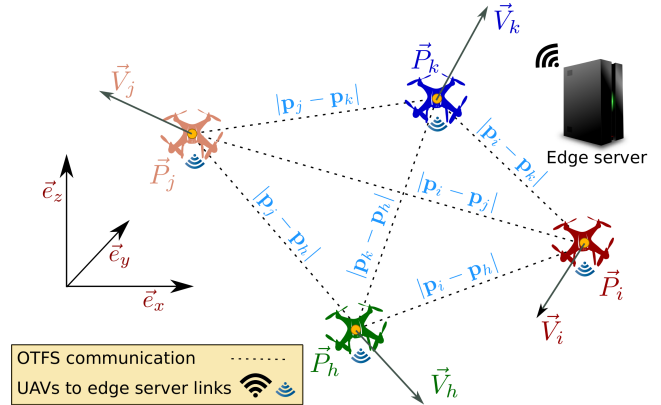


Fig. 1. Communicating UAVs assisted by an edge server. The  $n$ -th UAV has position  $\vec{P}_n$  and velocity  $\vec{V}_n$ , measured with respect to a common Cartesian coordinate system. The notation  $|\mathbf{p}_n - \mathbf{p}_m|$  denotes the distance between UAV  $n$  and UAV  $m$ , where  $\mathbf{p}_n$  and  $\mathbf{p}_m$  are the components of the geometric vectors  $\vec{P}_n$  and  $\vec{P}_m$ , respectively.

estimating the time-delay of pilot signals' propagation. Despite the extensive research into using orthogonal frequency-division multiplexing (OFDM) waveforms for this purpose [5], [6], the challenge of achieving precise localization in non-line-of-sight (nLoS) and high-mobility scenarios persists [7]. To address this, orthogonal time-frequency space (OTFS) has been explored as an alternative to OFDM. In particular, [8] demonstrates the effectiveness of OTFS-modulated physical random access channel (PRACH) transmissions for time-of-arrival-based ranging, while [7] designs an OFTS transceiver for transmission and reception of positioning reference signals, using it for belief propagation-based cooperative positioning.

**Our Contribution.** In this work, we focus on a scenario (shown in Fig. 1) involving a UAV swarm where nodes communicate with each other as well as with an edge server, via OTFS-modulated signals that exploit the delay-Doppler representation of the channels [9]. Unlike prior research, our approach envisions achieving precise localization and velocities of all UAVs within the swarm without depending on the overhead of additional positioning signaling and exploiting the delay-Doppler domain channel estimation used by OTFS communication system. The time difference of arrival (TDoA) between line-of-sight (LoS) and nLoS paths is extracted from the delay domain enabling the UAVs to operate without the need for fine-grained sample-level synchronization (within  $1/B$  [s] for a communication bandwidth  $B$ ). The Doppler shifts of each path from the Doppler domain channel estimate enable to derive the corresponding UAVs velocities.

Low-resolution estimates of the delays in the channels between all pairs of UAVs are transmitted to the edge server,

which then associates these delay values with the identities of the UAVs. To accomplish this, we employ belief propagation (BP), a method known for its low complexity and flexibility, which has proven effective in solving localization problems [10], [11]. The edge server subsequently uses this information to estimate the UAVs' positions, applying a gradient descent algorithm that converges to the actual values of the UAVs' positions. It is worth noting that the edge server can be considered as one of the nodes participating in the localization process.

Importantly, the solution we propose, called *turbo-iterative positioning* (TIP), exhibits limited complexity and does not require the availability of extensive bandwidth, often required for precise localization. Moreover, by utilizing real-world traces, we demonstrate that TIP yields highly accurate estimated positions and velocities, and showcases resilience to noise, nearing the Cramer-Rao bound.

*Paper Organization.* The rest of the paper is organized as follows. In Sec. II, after detailing the assumptions and the problem formulation, we provide a roadmap to our solution, i.e., the TIP algorithm. The fundamental blocks of this algorithm are detailed in Secs. III–VI. Specifically, Sec. III describes how to map the channel delay profiles to the UAV identities, whereas Sec. IV and Sec. V describe the proposed estimators for the UAV's positions and velocities, respectively. Then, Sec. VI combines the previous results in a highly efficient positioning algorithm, and Sec. VII presents the joint Cramér Rao lower bound on the variance of the position-velocity estimator. Finally, we numerically analyse the performance of our algorithm in Sec. VIII. Conclusions and future research directions are discussed in Sec. IX.

*Notations.* We denote *geometric vectors* by capital letters with an arrow on top, such as  $\vec{A}$ . Boldface uppercase and lowercase letters denote matrices and vectors, respectively. The transpose of matrix  $\mathbf{A}$  is denoted by  $\mathbf{A}^T$ , whereas  $[\mathbf{A}]_{i,j}$  indicates its  $(i,j)$ -th element.  $\mathbf{I}$  is the identity matrix and the L2-norm of the vector  $\mathbf{a}$  is represented by  $|\mathbf{a}|$ . Given a Cartesian coordinate system with basis vectors  $\vec{e}_x$ ,  $\vec{e}_y$ , and  $\vec{e}_z$ , the geometric vector  $\vec{A}$  is represented as a three-dimensional column vector  $\mathbf{a} = [\langle \vec{A}, \vec{e}_x \rangle, \langle \vec{A}, \vec{e}_y \rangle, \langle \vec{A}, \vec{e}_z \rangle]^T$ . Sets, lists, or maps are denoted by calligraphic or Greek capital letters. The estimate of the quantity  $a$  is denoted by  $\hat{a}$ . The probability of an event  $A$  is referred to as  $\mathbb{P}(A)$ , while the probability density function (pdf) of the random variable  $a$  is denoted by  $f_a(a)$ . The symbol  $\mathbb{E}_a[\cdot]$  stands for expectation with respect to the random variable  $a$ . Finally, the Gaussian distribution with zero mean and variance  $\sigma^2$  is denoted by  $\mathcal{N}(0, \sigma^2)$  and the uniform distribution between  $a$  and  $b$  is denoted by  $\mathcal{U}[a, b]$ .

## II. SYSTEM MODEL AND PROBLEM STATEMENT

We consider a swarm of  $N$  UAVs located in a 3D flight area. The position and the velocity of the generic UAV  $i$  ( $i=1, \dots, N$ ) are denoted by the geometric vectors  $\vec{P}_i$  and  $\vec{V}_i$ , respectively, which refer to a common Cartesian coordinate system. We also use the symbol  $\mathbf{p}_i = [p_{i,x}, p_{i,y}, p_{i,z}]^T$  to denote the components of  $\vec{P}_i$  along the  $x$ ,  $y$ , and  $z$  axis of the coordinate system and, similarly,  $\mathbf{v}_i = [v_{i,x}, v_{i,y}, v_{i,z}]^T$  to

denote the components of the velocity vector  $\vec{V}_i$ . A subset of  $A$  UAVs acts as *anchors*<sup>1</sup> for the system, i.e., their positions and velocities are perfectly known while the positions and velocities of the remaining  $\bar{N} = N - A$  UAVs are unknown and have to be estimated. Note that four anchors are sufficient to resolve translation and rotation ambiguities while estimating the UAVs' positions.

As depicted in Fig. 1, the UAVs communicate with each other, as well as with an edge server controlling the geographical area of interest, using the OTFS modulation. The wireless channel connecting any two UAVs presents high-mobility multipath fading characteristics. For simplicity, we assume that no physical obstacle, other than the UAVs belonging to the swarm, can reflect or block the signal. Thus, each communication channel between any pair of UAVs is characterized by the LoS path and  $N - 2$  nLoS components due to a single reflection from each of the other UAVs in the swarm. Then the time-delay expression of the channel connecting UAVs  $i$  and  $j$  ( $j \neq i$ ) is given by [9]:

$$h_{i,j}(t, \tau) = \sum_{k=1, k \neq i}^N c_{i,j,k} e^{j2\pi \nu_{i,j,k} t} \delta(\tau - \tau_{i,j,k}) \quad (1)$$

where  $c_{i,j,k}$ ,  $\tau_{i,j,k}$ , and  $\nu_{i,j,k}$  are, respectively, the channel coefficients, the path delay, and the Doppler shifts generated by the signal reflection on the  $k$ -th UAV. When  $k=j$ , we have the *LoS* path, otherwise we have the *nLoS*. We assume that the pilot power is sufficient for the channel estimation units of all OTFS receivers to identify all the paths parameters in (1).

In a practical scenario where the UAVs' transceivers are not synchronized with respect to a common time reference, they align onto the LoS path, which is associated with the zero delay in the delay-Doppler domain. Then, the delay  $\tau_{i,j,k}$  corresponds to the TDoA between the  $k$ -th nLoS path and the LoS path, and it is given by (see Fig. 1)

$$\tau_{i,j,k} = \tau_{j,k} + \tau_{k,i} - \tau_{i,j} \quad (2)$$

where  $\tau_{n,m} = \frac{1}{c} |\mathbf{p}_n - \mathbf{p}_m|$ ,  $n, m \in \{i, j, k\}$ , is the signal propagation delay from UAV  $n$  to UAV  $m$ , and  $c$  is the speed of light. Clearly,  $\tau_{i,j,j} = 0$  by definition.

Delays  $\tau_{i,j,k}$  depend upon the swarm geometry and, for each one of them, we define the corresponding distance<sup>2</sup>

$$\delta_{i,j,k} \triangleq c \tau_{i,j,k} = |\mathbf{p}_j - \mathbf{p}_k| + |\mathbf{p}_k - \mathbf{p}_i| - |\mathbf{p}_i - \mathbf{p}_j|. \quad (3)$$

Notice also that, due to channel reciprocity,  $\delta_{i,j,k} = \delta_{j,i,k} \forall i, j$ , and  $k \neq \{i, j\}$ . The delays  $\tau_{i,j,k}$  or, equivalently, the distances in (3) can be measured through pilot-based OTFS channel estimation techniques ([12]) to a degree of accuracy dependent upon the signal bandwidth  $B$ .

The Doppler shifts  $\nu_{i,j,k}$  are instead functions of both UAV's velocities and positions. For each of them, we define the

<sup>1</sup>For simplicity we refer to the anchors as UAVs; however, they can also be stationary ground nodes.

<sup>2</sup>We refer to this as distance for convenience; more precisely, it is the difference in length between nLoS and LoS paths.

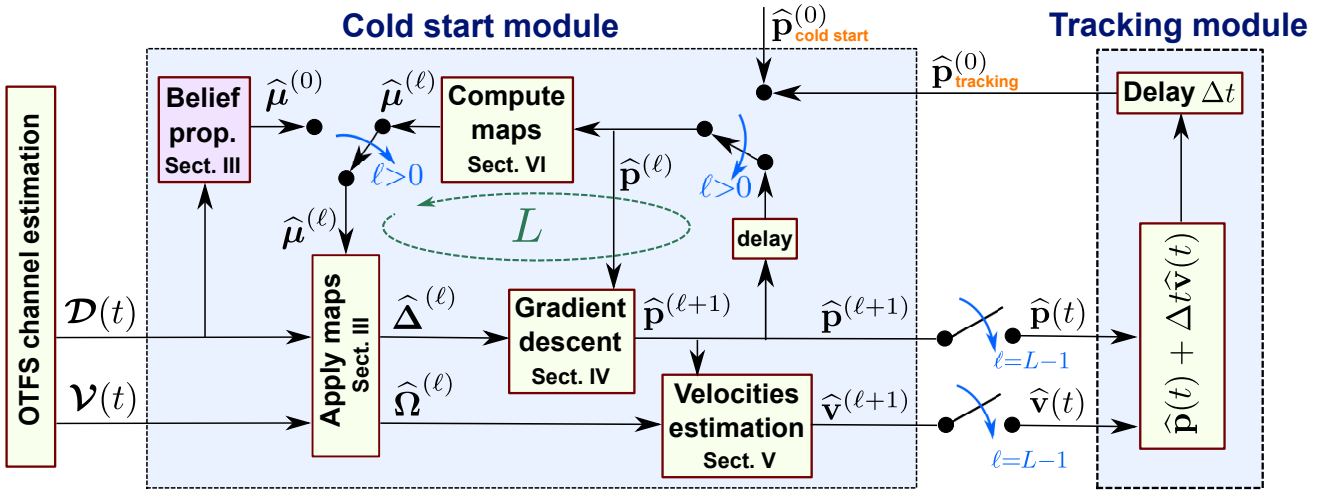


Fig. 2. Scheme of the TIP algorithmic framework. The switch on the left-hand side of the Cold start module remains in place for all  $\ell \geq 0$  in the Tracking mode, since the Belief propagation block is unused.

TABLE I  
SUMMARY OF VARIABLES AND PARAMETERS

Symbol	Description
$N$	Total number of UAVs
$A$	Number of anchor UAVs
$f_c, B$	Signal central frequency and bandwidth
$T_f$	OTFS frame duration
$M_d, N_D$	Number of delay and Doppler bins
$\mathbf{p}_i, \mathbf{v}_i$	Components of the position and velocity vectors of the $i$ -th UAV
$\tau_{i,j,k}$	TDoA between the $k$ -th non-LoS path and the LoS path, when UAV $j$ communicates with UAV $i$
$\delta_{i,j,k}$	Distance corresponding to the propagation delay $\tau_{i,j,k}$
$\tilde{\delta}_{i,j,k}$	Discretized distance $\delta_{i,j,k}$
$\nu_{i,j,k}$	Doppler shift of the signal transmitted by UAV $j$ , reflected by UAV $k$ , and received at UAV $i$
$\omega_{i,j,k}$	Velocity corresponding to the Doppler shift $\nu_{i,j,k}$
$\tilde{\omega}_{i,j,k}$	Discretized velocity $\omega_{i,j,k}$
$\mathcal{D}_{i,j}, \mathcal{V}_{i,j}$	Lists describing the profile of the channel connecting UAV $i$ and UAV $j$
$\mu_{i,j}$	Map associating the elements of $\mathcal{D}_{i,j}$ and $\mathcal{V}_{i,j}$ to the UAV's identities

corresponding velocity,  $\omega_{i,j,k} \triangleq \frac{c}{f_c} \nu_{i,j,k}$ , which, as shown in Appendix A, can be written as:

$$\omega_{i,j,k} = (\mathbf{v}_j - \mathbf{v}_k)^\top \mathbf{u}_{j,k}(\mathbf{p}) + (\mathbf{v}_k - \mathbf{v}_i)^\top \mathbf{u}_{k,i}(\mathbf{p}). \quad (4)$$

where  $\mathbf{p} = [\mathbf{p}_1^\top, \dots, \mathbf{p}_N^\top]^\top$  is a column vector of size  $3N$  stacking all components of the position vectors  $\tilde{P}_i$  ( $i=1, \dots, N$ ),  $f_c$  is the signal frequency, and the elements of

$$\mathbf{u}_{n,m}(\mathbf{p}) = \frac{\mathbf{p}_n - \mathbf{p}_m}{|\mathbf{p}_n - \mathbf{p}_m|} \quad (5)$$

are the components of the versor pointing from UAV  $m$  to UAV  $n$ .

In OTFS, the delay Doppler (DD) domain is discretized into an  $M_d \times N_D$  grid resulting in a delay resolution of  $\Delta\tau = \frac{T}{M_d} = \frac{1}{B}$  and a Doppler shift resolution of  $\Delta\nu = \frac{1}{N_D T}$ , where  $T = \frac{1}{\Delta f}$  is the duration of a block in the frame of duration  $T_f = N_D T$  and  $B = M_d \Delta f$  is the communication

channel bandwidth [9]. Simple channel estimation techniques, such as the one in [12], enable estimating the delay and Doppler shift of each path with the above resolution. By partitioning the DD domain grid into disjoint rectangular tiles, UAVs can simultaneously broadcast a pilot in a single frame, thus allowing all the receivers to perform channel estimation simultaneously within  $T_f$  seconds [9]. Here we assume that the multipath channel exhibits fractional delays and Doppler shifts, and that, for each delay, there is only one Doppler shift<sup>3</sup>. In turn, this allows estimating the distances  $\delta_{i,j,k}$  and the velocities  $\omega_{i,j,k}$  from the measurements

$$\tilde{\delta}_{i,j,k} = \delta_{i,j,k} + \eta_{i,j,k} \quad (6)$$

$$\tilde{\omega}_{i,j,k} = \omega_{i,j,k} + \zeta_{i,j,k} \quad (7)$$

where  $\eta_{i,j,k}$  and  $\zeta_{i,j,k}$  are the errors affecting, respectively, distance and velocity estimation. These errors are due to the quantization noise caused by the limited DD resolutions  $\Delta\tau$  and  $\Delta\nu$  as well as the effect of thermal noise. While the thermal noise component contributing to  $\eta_{i,j,k}$  and  $\zeta_{i,j,k}$  can be reduced by increasing the pilot power [12], the quantization noise can only be reduced at the greater cost of increasing the bandwidth  $B$  and the frame length  $T_f$ . Hence, in the following we assume that estimation errors are only due to quantization noise.

If the UAV's positions are unknown, the  $i$ -th UAV cannot associate each path in (1) with the identity of the UAV that generated it. Rather, it can only arrange the delays  $\tilde{\delta}_{i,j,k}$  in the list

$$\mathcal{D}_{i,j} = \{d_{i,j,m} | m = 1, \dots, N-1\} \quad (8)$$

and the velocities  $\tilde{\omega}_{i,j,k}$  in the list

$$\mathcal{V}_{i,j} = \{v_{i,j,m} | m = 1, \dots, N-1\} \quad (9)$$

where the elements of  $\mathcal{D}_{i,j}$  appear in increasing order (i.e.,  $d_{i,j,1} \leq d_{i,j,2} \leq \dots \leq d_{i,j,N-1}$ ) In general,  $d_{i,j,m} = \tilde{\delta}_{i,j,k}$ , and

<sup>3</sup>The latter assumption reflects the case where at most one scatterer falls within any ellipse with foci at the transmitter and receiver.

$v_{i,j,m} = \tilde{\omega}_{i,j,k}$ , if the elements at position  $m$  in both lists correspond to the DD signature of the  $k$ -th UAV. In other words, we can associate with each list  $\mathcal{D}_{i,j}$  and  $\mathcal{V}_{i,j}$  a bijective map of the indices

$$\mu_{i,j} : \{1, \dots, N-1\} \rightarrow \{1, \dots, N\} \setminus \{i\}$$

such that  $\mu_{i,j}(m) = k$ . Note that  $d_{i,j,1} = 0$  corresponds to the LoS path between UAV  $j$  and UAV  $i$ , since it is the shortest possible TDoA. By defining the set of lists  $\mathcal{D} \triangleq \{\mathcal{D}_{i,j} | i, j = 1, \dots, N, i \neq j\}$  and  $\mathcal{V} \triangleq \{\mathcal{V}_{i,j} | i, j = 1, \dots, N, i \neq j\}$ , and the set of maps  $\boldsymbol{\mu} \triangleq \{\mu_{i,j} | i, j = 1, \dots, N, i \neq j\}$ , the problem we address in this work can be stated as follows:

**Problem statement** – Given  $N$  UAVs communicating using OTFS through a channel as in (1), and the lists of noisy delay-Doppler profiles  $\mathcal{D}$  and  $\mathcal{V}$ , how can an edge server reliably estimate the UAVs' geometric positions and velocities vectors,  $\vec{P}_i$  and  $\vec{V}_i$ ,  $i = 1, \dots, N$ ?

**Solution Roadmap.** We answer this question by developing a new positioning algorithm called TIP (Turbo Iterative Positioning), schematized in Fig. 2. Using the TDoA and Doppler shift measurements of the OTFS channel estimation on all the UAVs links, collected in the set of lists  $\mathcal{D}$  and  $\mathcal{V}$  (resp.), TIP enables two operational modes: (i) *cold start* where no prior information on positions and velocities is available, and (ii) *tracking* where the estimated position and velocities are updated every  $\Delta t$  seconds using the previous estimates. The cold start module is iterative and runs a belief propagation algorithm to produce an initial estimate (at iteration  $\ell = 0$ ) of the maps  $\boldsymbol{\mu}$  assigning the identity of the scatterers in each path of each link. It then iterates  $L$  times to refine the initial random positions and the corresponding maps. At the core of the iterative loop of TIP, a gradient descent algorithm minimizes an error function to estimate the positions at step  $\ell + 1$ , given the currently estimated positions and maps. The same maps are applied to the lists of Doppler shifts  $\mathcal{V}$  to estimate the velocities. In the tracking mode, the estimates of positions and velocities are combined to predict the next position after  $\Delta t$  seconds, which can be used to re-initialize the cold start module without the need for the belief propagation block.

The overall TIP operation is detailed in Sec. VI and includes the following blocks:

- 1) *Belief Propagation* – provides an initial estimate of the maps  $\boldsymbol{\mu}$ , given the sets of lists  $\mathcal{D}$ . Towards this goal, we relax the deterministic maps  $\boldsymbol{\mu}$  to probabilistic maps  $\mathcal{M}$ , and use a BP approach to obtain an estimation of  $\hat{\boldsymbol{\mu}}$  (see Sec. III).
- 2) *Apply maps* – permutes the TDoA and Doppler shift lists  $\mathcal{D}$  and  $\mathcal{V}$  according to the estimated maps  $\hat{\boldsymbol{\mu}}$ , to produce the permuted lists  $\hat{\Delta}$  and  $\hat{\Omega}$ , respectively (see Sec. III-C).
- 3) *Gradient descent* – computes the UAVs' position estimates  $\hat{\mathbf{p}}$ , given the lists  $\hat{\Delta}$  from *Apply maps* (see Sec. IV).
- 4) *Velocity estimation* – provides estimates  $\hat{\mathbf{v}}$  of the UAV's velocities using the estimates  $\hat{\mathbf{p}}$ , and the set of lists  $\hat{\Omega}$  from *Apply maps* (see Sec. V).

- 5) *Compute maps* – computes the set of maps  $\hat{\boldsymbol{\mu}}$  corresponding to the current position estimates  $\hat{\mathbf{p}}$  (see Sec. VI).

### III. MAPPING DELAY PROFILES INTO UAVS' IDENTITIES

To associate channel observations with UAVs' identities, the edge server has to estimate the maps  $\boldsymbol{\mu}$ . Let us first focus on a subset of four UAVs, respectively labelled by  $i, j, k, h$ , as depicted in Fig. 1. The figure also highlights the actual distances  $|\mathbf{p}_n - \mathbf{p}_m|$  between the UAVs, for  $n, m \in \{i, j, k, h\}$ .

By recalling the expression of  $\delta_{i,j,k}$  in (3), it is easy to observe that for all quadruples of UAVs in the swarm, we have:

$$\delta_{i,j,k} - \delta_{i,j,h} + \delta_{i,k,h} - \delta_{j,h,k} = 0 \quad (10)$$

where  $i, j, k, h \in \{1, \dots, N\}$ ,  $j \neq i$ ,  $k \neq \{i, j\}$ ,  $h \neq \{i, j, k\}$ . This implies that one can find the correct associations  $\mu_{i,j}$  between the entries of the list  $\mathcal{D}_{i,j}$  and the UAVs' identities by searching through the elements of lists  $\mathcal{D}_{i,j}$ ,  $\mathcal{D}_{i,k}$ , and  $\mathcal{D}_{j,h}$ , until a relation such as the one in (10) holds. More precisely, given the ordered lists  $\mathcal{D}_{i,j}$ ,  $\mathcal{D}_{i,k}$ , and  $\mathcal{D}_{j,h}$ , if for some integers  $m, n, s, t \in \{1, \dots, N-1\}$  and such that  $m \neq n$ , the following relation holds in the absence of noise:

$$d_{i,j,m} - d_{i,j,n} + d_{i,k,s} - d_{j,h,t} = 0, \quad (11)$$

then, by comparing (10) to (11), we can deduce the maps  $\mu_{i,j}(m) = k$ ,  $\mu_{i,j}(n) = h$ ,  $\mu_{i,k}(s) = h$ , and  $\mu_{j,h}(t) = k$ .

It is worth noting that there are  $O(N^8)$  constraint equations like (11) that need to be satisfied simultaneously by the  $d$ 's in all the lists  $\mathcal{D}$ , and a brute force search would have an exponential complexity of  $O([(N-1)!]^{N(N-1)})$ . Additionally, whenever the distances  $\delta_{i,j,k}$  are affected by noise, the left hand side of (11) is, in general, not 0.

To find the maps in the presence of noise in an efficient way, we relax the deterministic maps  $\boldsymbol{\mu}$  to probabilistic maps  $\mathcal{M} \triangleq \{\mathcal{M}_{i,j} | i, j = 1, \dots, N, i \neq j\}$  where the  $m$ -th element of the map  $\mathcal{M}_{i,j}(m)$  has probability mass function (pmf)  $\pi_{i,j,m,k} \triangleq \mathbb{P}(\mathcal{M}_{i,j}(m) = k)$  for  $k \in \{1, \dots, N\} \setminus \{i\}$ . In the absence of quantization noise,  $\eta_{i,j,k}$ , the pmf of  $\mathcal{M}_{i,j}(m)$  coincides with a distribution taking on 1 in correspondence of the actual value  $\mu_{i,j}(m)$ . To derive accurate estimates  $\hat{\boldsymbol{\mu}}_{i,j}$  of the maps  $\mu_{i,j}$ , we should solve the problem

$$\hat{\boldsymbol{\mu}} = \arg \max_{\boldsymbol{\mu}} \mathbb{P}(\mathcal{M} = \boldsymbol{\mu}) \quad (12)$$

which still has a complexity  $O([(N-1)!]^{N(N-1)})$  and it is in any case intractable since the joint pmf of  $\mathcal{M}$  is unknown. To overcome this problem, we propose the heuristic greedy approach described in Algorithm 2, which relies on the marginals  $\pi_{i,j,m,k}$  and has polynomial complexity  $O(N(N-1)(N-2))$ . Specifically, we first show how to compute such marginals using a BP approach, and then we describe how to estimate the maps  $\boldsymbol{\mu}$ , given the marginals  $\pi_{i,j,m,k}$ .

### A. Computing the marginals $\pi_{i,j,m,k}$

To compute the marginals  $\pi_{i,j,m,k}$ , we rely on the property (11), which holds for every quadruple of nodes. However, first we need to consider some special cases of (11), which must be treated separately. Specifically, we observe that, when  $m=1$ , the first term of (11) is  $d_{i,j,1}=0$  by definition, since it is the smallest possible TDoA and, thus, it refers to the LoS path<sup>4</sup>, i.e., the path connecting node  $j$  with node  $i$ . It follows that  $\mu_{i,j}(1)=j$ , which also implies  $k=j$ . In this case, (10) becomes meaningless since its left hand side is identically zero. Similarly, we deduce  $\mu_{i,k}(1)=k$  when  $s=1$  and  $\mu_{j,h}(1)=h$  when  $t=1$ . Summarizing, for all  $i \neq j$ , we can handle these special cases by setting  $\pi_{i,j,1,k}=1$  for  $k=j$  and 0 for  $k \neq \{i, j\}$ .

To compute the other marginals, we use (11) and apply a BP approach but considering the indices  $m, n, s, t$ , with  $m \neq n$  ranging in  $\{2, \dots, N-1\}$  only. Also, in the following analysis we assume  $i \neq j$ ,  $k \neq \{i, j\}$ , and  $h \neq \{i, j, k\}$ , since we work on a quadruple  $\{i, j, k, h\}$ .

In the BP terminology, the random maps  $\mathcal{M}_{i,j}$  represent the *variable nodes*, whereas the *check nodes* are defined from (11) by the equations

$$d_{i,j,\mathcal{M}_{i,j}^{-1}(k)} - d_{i,j,\mathcal{M}_{i,j}^{-1}(h)} + d_{i,k,\mathcal{M}_{i,k}^{-1}(h)} - d_{j,h,\mathcal{M}_{j,h}^{-1}(k)} = 0 \quad (13)$$

which specify the variable nodes involved in the check node. Further, in the BP model, the marginals,  $\pi_{i,j,m,k}$ , represent the messages flowing from the variable nodes,  $\mathcal{M}_{i,j}$ , to the check nodes.

The messages  $Z^{i,j,m}$  from check nodes to variable nodes are defined by the left hand side of (13), i.e.,

$$Z^{i,j,m} = d_{i,j,m} - X_1 + X_2 - X_3 \quad (14)$$

for any  $i, j=1, \dots, N$ ,  $i \neq j$ , and  $m=2, \dots, N-1$ , where  $X_1$ ,  $X_2$ , and  $X_3$  are discrete random variables taking on values as follows:  $x_1 \in \mathcal{D}_{i,j} \setminus \{d_{i,j,m}, d_{i,j,1}\}$ ,  $x_2 \in \cup_{u \neq \{i,j\}} \mathcal{D}_{i,u} \setminus \{d_{i,u,1}\}$ , and if  $x_2$  has been selected from  $\mathcal{D}_{i,\ell}$  for some  $\ell$ , then  $x_3 \in \cup_{u \neq \{i,\ell\}} \mathcal{D}_{j,u} \setminus \{d_{j,u,1}\}$ . It is clear that  $X_2$  and  $X_3$  are correlated, while  $X_1$  is independent of both  $X_2$  and  $X_3$ .

Next, for  $m, n, s, t \in \{2, \dots, N-1\}$ , and  $m \neq n$ , let us define the events

$$\begin{aligned} A_{k,h,n,s,t}^{i,j} &= \{\mathcal{M}_{i,j}(n)=h, \mathcal{M}_{i,k}(s)=h, \mathcal{M}_{j,h}(t)=k\}, \\ B_{k,h,n,s,t}^{i,j,m} &= \{\mathcal{M}_{i,j}(m)=k, A_{k,h,n,s,t}^{i,j}\}. \end{aligned}$$

Then, by conditioning on the events  $B_{k,h,n,s,t}^{i,j,m}$ , the density of  $Z^{i,j,m}$  is given by:

$$\begin{aligned} f(z^{i,j,m}) &= \sum_{\substack{k \neq \{i,j\}, h \neq k \\ n,s,t=2,\dots,N-1 \\ n \neq m}} f(z^{i,j,m} | B_{k,h,n,s,t}^{i,j,m}) \mathbb{P}(B_{k,h,n,s,t}^{i,j,m}) \\ &= \sum_{\substack{k \neq \{i,j\}, h \neq k \\ n,s,t=2,\dots,N-1 \\ n \neq m}} g(z_{k,h,n,s,t}^{i,j,m}) \mathbb{P}(B_{k,h,n,s,t}^{i,j,m}) \quad (15) \end{aligned}$$

<sup>4</sup>We recall that quantization applied to small TDoAs may result in more than one zero entries in the lists  $\mathcal{D}_{i,j}$ . Since these entries are indistinguishable, we arbitrarily associate the LoS path with one of them, randomly chosen.

where  $z_{k,h,n,s,t}^{i,j,m}$  is the left hand side of (11) and  $g(\cdot)$  is a distribution accounting for the sum of 4 independent quantization errors characterized by the uniform distribution  $f_\eta(\cdot)$  with support in  $[-\frac{c}{2B}, \frac{c}{2B}]$ . Hence,  $g(\cdot) = f_\eta(\cdot) * f_\eta(\cdot) * f_\eta(\cdot) * f_\eta(\cdot)$  with  $*$  denoting the convolution operator. The above definition of  $g(\cdot)$  can be explained by the fact that (14) is a sum of four quantized values of actual TDoAs, which are unknown, but within the quantization intervals. Due to the rounding operation, the quantization error is deterministically dependent upon the actual value of a TDoA, but the uncertainty of such a value can be translated onto the uniform distribution  $f_\eta(\cdot)$  centered around the center point of a quantization interval for the  $\eta$ 's to represent a random quantization noise.

The messages from the check nodes to the variable nodes are the conditional probabilities

$$\begin{aligned} p_{i,j,m,k} &\triangleq \mathbb{P}(\mathcal{M}_{i,j}(m) = k | z^{i,j,m}) \\ &= \frac{f(z^{i,j,m} | \mathcal{M}_{i,j}(m) = k) \cdot \pi_{i,j,m,k}}{f(z^{i,j,m})} \\ &\approx \frac{\pi_{i,j,m,k}}{f(z^{i,j,m})} \sum_{\substack{h \neq \{i,j,k\} \\ n,s,t=2,\dots,N-1 \\ n \neq m}} g(z_{k,h,n,s,t}^{i,j,m}) \cdot \pi_{i,j,n,h} \cdot \pi_{i,k,s,h} \cdot \pi_{j,h,t,k} \quad (16) \end{aligned}$$

where

$$f(z^{i,j,m} | \mathcal{M}_{i,j}(m) = k) = \sum_{\substack{h \neq \{i,j,k\} \\ n,s,t=2,\dots,N-1}} g(z_{k,h,n,s,t}^{i,j,m}) \mathbb{P}(A_{h,n,s,t}^{i,j})$$

and, in the last line of (16), we assumed independence among the events  $\mathcal{M}_{i,j}(n)=h$ ,  $\mathcal{M}_{i,k}(s)=h$ , and  $\mathcal{M}_{j,h}(t)=k$ , so that  $\mathbb{P}(A_{h,n,s,t}^{i,j}) \approx \pi_{i,j,n,h} \cdot \pi_{i,k,s,h} \cdot \pi_{j,h,t,k}$ .

The iterative procedure that leads to the computation of the probabilities  $\pi_{i,j,m,k}$  is described in Algorithm 1. For the  $\ell$ -th iteration and for  $m=2, \dots, N-1$ , based on (16) we compute, up to a scaling factor

$$p_{i,j,m,k}^{(\ell)} \propto \sum_{\substack{h \neq \{i,j,k\} \\ n,s,t=2,\dots,N-1 \\ n \neq m}} g(z_{k,h,n,s,t}^{i,j,m}) \cdot \pi_{i,j,n,h}^{(\ell-1)} \cdot \pi_{i,k,s,h}^{(\ell-1)} \cdot \pi_{j,h,t,k}^{(\ell-1)}, \quad (17)$$

and then normalize it as

$$\pi_{i,j,m,k}^{(\ell)} = \frac{p_{i,j,m,k}^{(\ell)}}{\sum_{u \neq \{i,j\}} p_{i,j,m,u}^{(\ell)}} \quad (18)$$

where  $\pi_{i,j,m,k}^{(0)}$  is initialized to  $\frac{1}{N-2}$ , for  $m=2, \dots, N-1$ .

In order to use only the *extrinsic information* provided by the other marginals, in (17) we removed the term  $\pi_{i,j,m,k}^{(\ell-1)}$  appearing in (16), since it provides highly correlated information with  $p_{i,j,m,k}^{(\ell)}$ . Once the BP algorithm reaches convergence or a sufficient number of iterations has been performed, the resulting marginal pmf's,  $\pi_{i,j,m,k}$  are fed to Algorithm 2.

### B. Estimating the maps $\mu$ given the marginals $\pi_{i,j,m,k}$

For each pair of UAVs,  $(i, j)$ , we collect the marginals  $\pi_{i,j,m,k}$  in the  $(N-1) \times N$  matrix  $\mathbf{\Pi}$ . We then work iteratively and, at each step, we find the most likely association in

the map. Specifically, we seek the largest entry of  $\mathbf{\Pi}$ , we record its row index  $m'$  and its column index  $k'$ , and we set  $\widehat{\mu}_{i,j}(m')=k'$ . Next, we set the  $m'$ -th row and the  $k'$ -th column of  $\mathbf{\Pi}$  to zero: this operation is necessary because no other element of the map can be assigned to value  $k'$  in the following steps of the algorithm. The procedure ends when all values of the elements of  $\mathbf{\Pi}$  become zero, i.e., a decision is made on all the elements of the map  $\widehat{\mu}_{i,j}$ . The procedure is detailed in Algorithm 2.

### C. Applying the estimated maps to lists $\mathcal{D}$ and $\mathcal{V}$

Once the estimated map  $\widehat{\mu}_{i,j}$  is available, it can be applied to lists  $\mathcal{D}_{i,j}$  and  $\mathcal{V}_{i,j}$  in order to associate to each reflecting UAV,  $k$ , an estimate of the distance  $\delta_{i,j,k}$  and of the velocity  $\omega_{i,j,k}$ . We recall that the lists  $\mathcal{D}_{i,j}$  and  $\mathcal{V}_{i,j}$  are defined in (8) and (9), respectively.

Specifically, the distance associated with the  $k$ -th path is estimated as  $\widehat{\delta}_{i,j,k}=d_{i,j,\widehat{m}}$  where  $\widehat{m}=\widehat{\mu}_{i,j}^{-1}(k)$ , and  $d_{i,j,\widehat{m}}$  is an element of the list  $\mathcal{D}_{i,j}$ . Similarly, the velocity associated with the  $k$ -th path is estimated as  $\widehat{\omega}_{i,j,k}=v_{i,j,\widehat{m}}$  where  $v_{i,j,\widehat{m}}$  is an element of the list  $\mathcal{V}_{i,j}$ . This procedure is represented by the block labelled ‘‘Apply maps’’, shown in Fig. 2.

---

#### Algorithm 1 $\{\pi_{i,j,m,k}\} = \text{ComputeMarginals}(\mathcal{D})$

---

**Require:**  $N, \mathcal{D}, I_\mu > 0$

```

for  $i, j = 1, \dots, N, j \neq i$  do
   $\pi_{i,j,1,k}^{(0)} \leftarrow -1$ , for  $k=j$  and  $\pi_{i,j,1,k}^{(0)} \leftarrow 0$  for  $k \neq \{i, j\}$ 
   $\pi_{i,j,m,k}^{(0)} \leftarrow \frac{1}{N-2}$ , for  $m=2, \dots, N-1$ , and  $k \neq \{i, j\}$ 
for  $\ell=1, \dots, I_\mu$  do
  for  $i, j=1, \dots, N, j \neq i, m=2, \dots, N-1$  do
    for  $k=1, \dots, N, k \neq \{i, j\}$  do
      compute  $p_{i,j,m,k}^{(\ell)}$  using (17)
    for  $k=1, \dots, N, k \neq \{i, j\}$  do
      compute  $\pi_{i,j,m,k}^{(\ell)}$  using (18)
return  $\{\pi_{i,j,m,k}^{(I_\mu)}\}$ 

```

---



---

#### Algorithm 2 $\widehat{\mu} = \text{EstimateMaps}(\mathcal{D})$

---

**Require:**  $N, \mathcal{D}$

```

 $\{\pi_{i,j,m,k}\} \leftarrow \text{ComputeMarginals}(\mathcal{D})$ 
for  $i, j = 1, \dots, N, i \neq j$  do
   $[\mathbf{\Pi}]_{m,k} \leftarrow \begin{cases} \pi_{i,j,m,k} & k \neq i \\ 0 & k = i \end{cases}$ 
  while  $\mathbf{\Pi} \neq \mathbf{0}$  do
     $[m', k'] \leftarrow \arg \max_{m,k} ([\mathbf{\Pi}]_{m,k})$ 
     $\widehat{\mu}_{i,j}(m') \leftarrow k'$ 
     $[\mathbf{\Pi}]_{m',q} \leftarrow 0$  for  $q=1, \dots, N$ 
     $[\mathbf{\Pi}]_{q,k'} \leftarrow 0$  for  $q=1, \dots, N-1$ 
return  $\widehat{\mu}$ 

```

---

## IV. ESTIMATING THE NODE POSITIONS

The estimates  $\widehat{\mu}$  of the maps  $\mu$  can be used by the edge server to associate the elements of the lists  $\mathcal{D}$  with the UAVs that generated them. In the case of perfect maps estimates, the

edge server is able to retrieve the channel observations  $\widetilde{\delta}_{i,j,k}$  in their correct ordering. To estimate the UAV’s positions, we apply the gradient descent (GD) algorithm so as to minimize the square error,  $\mathcal{E}$ , between  $\widetilde{\delta}_{i,j,k}$  and the tentative channel observations  $\theta_{i,j,k}$ .

More precisely, let  $\mathbf{t}_i = [t_{i,x}, t_{i,y}, t_{i,z}]^\top$  be a tentative decision for the position of UAV  $i$ ,  $\mathbf{p}_i$ , and let  $\mathbf{t} \triangleq [\mathbf{t}_1^\top, \dots, \mathbf{t}_N^\top]^\top$ . Then, an estimate  $\widehat{\mathbf{p}}$  of the actual components  $\mathbf{p}$  can be obtained by solving the problem

$$\widehat{\mathbf{p}} = \arg \min_{\mathbf{t}} \mathcal{E}(\mathbf{t}) \quad (19)$$

where

$$\mathcal{E}(\mathbf{t}) \triangleq \sum_{i=1}^N \sum_{j=1}^N \sum_{\substack{k=1 \\ j \neq i, k \neq i, j}}^N \left( \widetilde{\delta}_{i,j,k} - \theta_{i,j,k}(\mathbf{t}) \right)^2 \quad (20)$$

is the square error between the channel observations,  $\widetilde{\delta}_{i,j,k}$ , and the tentative distances  $\theta_{i,j,k}(\mathbf{t}) \triangleq |\mathbf{t}_j - \mathbf{t}_k| + |\mathbf{t}_k - \mathbf{t}_i| - |\mathbf{t}_j - \mathbf{t}_i|$  according to (3). The square error in (20) is, in general, a non-convex function, nevertheless local or global minima can be easily found by applying a standard GD method.

In the GD algorithm, let  $\mathbf{t}^{(\alpha)}$  be the tentative positions at iteration  $\alpha \geq 0$ . Then, after applying one GD step, the tentative estimated position at iteration  $\alpha + 1$  is updated as  $\mathbf{t}^{(\alpha+1)} = \mathbf{t}^{(\alpha)} - \gamma^{(\alpha)} \mathbf{g}^{(\alpha)}$  where  $\gamma^{(\alpha)}$  denotes the step size,  $\mathbf{g} \triangleq \frac{\partial \mathcal{E}}{\partial \mathbf{t}}(\mathbf{t})$  is the gradient of  $\mathcal{E}(\mathbf{t})$  and  $\mathbf{g}^{(\alpha)} = \mathbf{g}|_{\mathbf{t}=\mathbf{t}^{(\alpha)}}$ . The step size can be kept constant or selected at each iteration according to some rule as, e.g., the Barzilai-Borwein method, where  $\gamma^{(\alpha)}$  is computed exploiting the trend of the most recent two iterations [13]. Let  $\mathbf{g} \triangleq [\mathbf{g}_1^\top, \dots, \mathbf{g}_N^\top]^\top$ . Then  $\mathbf{g}_h$  is given by

$$\mathbf{g}_h(\mathbf{t}) = \frac{\partial \mathcal{E}(\mathbf{t})}{\partial \mathbf{t}_h} = -2 \sum_{i=1}^N \sum_{j=1}^N \sum_{\substack{k=1 \\ j \neq i, k \neq i, j}}^N w_{i,j,k}(\mathbf{t}) \frac{\partial \theta_{i,j,k}(\mathbf{t})}{\partial \mathbf{t}_h} \quad (21)$$

where  $w_{i,j,k}(\mathbf{t}) \triangleq \widetilde{\delta}_{i,j,k} - \theta_{i,j,k}(\mathbf{t})$ . Since  $\frac{\partial |\mathbf{x}|}{\partial \mathbf{x}} = \frac{\mathbf{x}}{|\mathbf{x}|}$ , for any vector  $\mathbf{x}$ , using (3) we have

$$\frac{\partial \theta_{i,j,k}(\mathbf{t})}{\partial \mathbf{t}_h} = \begin{cases} \mathbf{u}_{i,k}(\mathbf{t}) - \mathbf{u}_{i,j}(\mathbf{t}) & \text{if } i = h \\ \mathbf{u}_{j,k}(\mathbf{t}) - \mathbf{u}_{j,i}(\mathbf{t}) & \text{if } j = h \\ \mathbf{u}_{k,i}(\mathbf{t}) + \mathbf{u}_{k,j}(\mathbf{t}) & \text{if } k = h \\ \mathbf{0} & \text{else} \end{cases} \quad (22)$$

where the versors  $\mathbf{u}_{n,m}$  are defined in (5). By using (22) in (21), we obtain

$$\mathbf{g}_h = -2 \begin{cases} \sum_{j \neq h} \sum_{k \neq h, j} w_{h,j,k}(\mathbf{u}_{h,k} - \mathbf{u}_{h,j}) & \text{if } i = h \\ \sum_{i \neq h} \sum_{k \neq i, h} w_{i,h,k}(\mathbf{u}_{h,k} - \mathbf{u}_{h,i}) & \text{if } j = h \\ \sum_{i \neq h} \sum_{j \neq i, h} w_{i,j,h}(\mathbf{u}_{h,i} + \mathbf{u}_{h,j}) & \text{if } k = h \end{cases}$$

By summing the above three contributions and renaming the summation indices, after some algebra we obtain

$$\mathbf{g}_h = 2 \sum_{\substack{i=1 \\ i \neq h}}^N \sum_{\substack{j=1 \\ j \neq h, i}}^N (w_{h,i,j} + w_{i,h,j})(\mathbf{u}_{h,i} - \mathbf{u}_{h,j}) - w_{i,j,h}(\mathbf{u}_{h,i} + \mathbf{u}_{h,j})$$

where, for simplicity, we omitted the dependency on  $\mathbf{t}$ . In our implementation, the GD algorithm starts from an initial

tentative value,  $\mathbf{t}^{(0)}$ , and iterates until the following stopping condition on the square error is satisfied:

$$\frac{\mathcal{E}(\mathbf{t}^{(\alpha+1)}) - \mathcal{E}(\mathbf{t}^{(\alpha)})}{\mathcal{E}(\mathbf{t}^{(\alpha)})} < \epsilon,$$

or a maximum number of iterations,  $I_\alpha$ , is reached. The initial tentative  $\mathbf{t}^{(0)}$  can be (i) chosen either as a prior estimate of the position, or (ii) randomly drawn. Case (i) is selected when TIP operates in tracking mode, or in cold start from the second TIP iteration onwards; case (ii) is selected only in cold start mode at the first TIP iteration.

#### A. Improving convergence to global optimum

Since the square error function  $\mathcal{E}(\mathbf{t})$  is not convex, the GD algorithm may reach a local minimum instead of the global one, thus leading to inaccurate positioning. To ensure convergence to the global minimum with high probability, we propose a heuristic method based on the following considerations. Consider that the GD algorithm has converged to its global minimum and that the minimizer of (20) is  $\mathbf{t}=\hat{\mathbf{p}}$ . Such estimate of the actual positions  $\mathbf{p}$  can be written as  $\hat{\mathbf{p}}=\mathbf{p}+\mathbf{e}$  where  $\mathbf{e}$  is the estimation error. Thus

$$\theta_{i,j,k}(\hat{\mathbf{p}}) = \theta_{i,j,k}(\mathbf{p}) + \psi_{i,j,k}$$

where, by definition,  $\theta_{i,j,k}(\mathbf{p})=\delta_{i,j,k}$  and  $\psi_{i,j,k}$  is the estimation error in the TDoA. Using (6), the term in the sum in (20) reduces to  $\tilde{\delta}_{i,j,k}-\theta_{i,j,k}(\hat{\mathbf{p}})=\eta_{i,j,k}-\psi_{i,j,k}$  where we recall that the terms  $\eta_{i,j,k}$  are the quantization errors on the channel observations. Thus, the square error at convergence is

$$\mathcal{E}(\hat{\mathbf{p}}) = \sum_{i=1}^N \sum_{\substack{j=1 \\ j \neq i}}^N \sum_{\substack{k=1 \\ k \neq i,j}}^N (\eta_{i,j,k} - \psi_{i,j,k})^2. \quad (23)$$

Since we assume that the global minimum of the function  $\mathcal{E}(\mathbf{t})$  has been reached at  $\mathbf{t}=\hat{\mathbf{p}}$ , any other choice for  $\mathbf{t}$  will lead to a larger square error. Consider now the choice  $\mathbf{t}=\mathbf{p}$ , which corresponds to  $\psi_{i,j,k}=0, \forall i, j, k$ . According to (23), we then have

$$\mathcal{E}(\hat{\mathbf{p}}) \leq \mathcal{E}(\mathbf{p}) = \sum_{i=1}^N \sum_{\substack{j=1 \\ j \neq i}}^N \sum_{\substack{k=1 \\ k \neq i,j}}^N \eta_{i,j,k}^2. \quad (24)$$

Now, given the actual position components,  $\mathbf{p}$ , the quantization errors,  $\eta_{i,j,k}$ , are deterministic quantities; however, as already observed, the uncertainty in  $\mathbf{p}$  can be translated into  $\eta_{i,j,k}$  being independent random variables with zero-mean, uniform distribution in the interval  $[-\frac{c}{2B}, \frac{c}{2B}]$  and, hence, variance  $\sigma_\eta^2 = \frac{c^2}{12B^2}$ . For sufficiently large  $N$  (that is, a sufficiently large number of observations  $\tilde{\delta}_{i,j,k}$ ), the following holds with high probability:

$$\mathcal{E}(\hat{\mathbf{p}}) \leq N(N-1)(N-2) \frac{c^2}{12B^2} \triangleq E_b. \quad (25)$$

In summary, when the GD algorithm converges to the global minimum, the residual square error is expected to be lower than  $E_b$ , whereas we expect  $\mathcal{E}(\hat{\mathbf{p}})$  to be much larger when it converges to a local minimum. Based on the above considerations, we improve the positioning accuracy of our algorithm

by comparing the square error  $\mathcal{E}(\hat{\mathbf{p}})$  at the output of the GD algorithm against the threshold  $\tilde{E}_b = \beta E_b$  where  $\beta > 1$  is a constant.

Referring to Fig. 2 the GD verifies the condition  $\mathcal{E}(\hat{\mathbf{p}}) > \tilde{E}_b$  at the  $L$ -th iteration. If it is not met the TIP is run again resetting  $\ell = 0$  and using a new randomly drawn  $\hat{\mathbf{p}}_{\text{cold start}}^{(0)}$ . This restart is repeated until  $\mathcal{E}(\hat{\mathbf{p}}) \leq \tilde{E}_b$ , or a maximum number of retries has been reached. Otherwise failure is declared. Note that the purpose of the constant  $\beta$  is to compensate for possible large statistical deviations of  $\mathcal{E}(\mathbf{p})$  (i.e., the r.h.s. of (24)) from  $E_b$ . As  $\beta$  decreases, the probability that reliable estimates are declared unreliable increases as well as the computational complexity of the algorithm. Conversely, as  $\beta$  increases, convergence to local minima are less likely to be detected and, in general, the positioning accuracy decreases.

*Remark 1:* The GD algorithm proposed above allows the joint estimation of the positions of all UAVs. However, we recall that only the positions of  $\bar{N}=N-A$  UAVs have to be estimated since the remaining  $A$  are anchors whose positions are perfectly known. To take this into account, the GD algorithm needs to be slightly modified as follows. Let  $\mathcal{A}$  be the set of anchor nodes. Then, for all  $i \in \mathcal{A}$ , the tentative decisions are set to the actual positions, i.e.,  $\mathbf{t}_i^{(0)}=\mathbf{p}_i$  and the gradient  $\mathbf{g}_i^{(\alpha)}$  is set to  $\mathbf{0}$  at every iteration step  $\alpha$ . This ensures  $\mathbf{t}_i^{(\alpha)}=\mathbf{p}_i$  for all iteration steps. The GD algorithm remains unchanged since the estimation error  $\mathbf{e}=\hat{\mathbf{p}}-\mathbf{p}$  is zero for all anchor nodes, while is (in general) non-zero for the others.

#### V. ESTIMATING THE NODES' VELOCITIES

Once the estimates of the UAVs' position vectors  $\hat{\mathbf{p}}$  and of the maps  $\hat{\boldsymbol{\mu}}$  are available, the components  $\mathbf{v}_i$  of the UAVs' geometric velocities  $\vec{V}_i, i=1, \dots, N$  can be estimated through (4). Indeed, from (4), we can write

$$\begin{aligned} \omega_{i,j,k} &= \mathbf{u}_{j,k}^\top \mathbf{v}_j + (\mathbf{u}_{k,i} - \mathbf{u}_{j,k})^\top \mathbf{v}_k - \mathbf{u}_{k,i}^\top \mathbf{v}_i \\ &= \mathbf{u}_{i,j,k}^\top \mathbf{v} \end{aligned} \quad (26)$$

where  $\mathbf{v}=[\mathbf{v}_1^\top, \dots, \mathbf{v}_N^\top]^\top$ . If we collect the terms  $\omega_{i,j,k}$  and  $\tilde{\omega}_{i,j,k}$  in the column vectors  $\boldsymbol{\omega}$  and  $\tilde{\boldsymbol{\omega}}$ , respectively, according to (7), we can write

$$\tilde{\boldsymbol{\omega}} = \boldsymbol{\omega} + \boldsymbol{\eta} = \mathbf{U}^\top \mathbf{v} + \boldsymbol{\zeta}. \quad (27)$$

where the columns of the matrix  $\mathbf{U}$  are  $\mathbf{u}_{i,j,k}$  and the elements of  $\boldsymbol{\zeta}$  are the discretization errors  $\zeta_{i,j,k}$ . The matrix  $\mathbf{U}$  has size  $3N \times N(N-1)^2$ , since  $N(N-1)^2$  is the total number of observations and  $3N$  is the total number of components of the velocity vectors.

Since the positions and velocities are known for the  $A$  anchors, the edge server only needs to estimate  $3\bar{N}$  parameters, with  $\bar{N}=N-A$ . In practice, if we let  $\bar{N}$  be the set of the UAVs which are not anchors, we just need to consider the reduced equation

$$\tilde{\boldsymbol{\omega}} = \bar{\mathbf{U}}^\top \bar{\mathbf{v}} + \boldsymbol{\zeta}, \quad (28)$$

instead of (27). In (28),  $\bar{\mathbf{U}}$  is a  $3\bar{N} \times N(N-1)^2$  matrix containing only the rows of  $\mathbf{U}$  corresponding to the UAVs in  $\bar{N}$  and, similarly,  $\bar{\mathbf{v}}$  has size  $3\bar{N}$  and contains only the contributions of the  $\bar{N}$  UAVs in  $\bar{N}$ .

We recall that  $\zeta$  represents the quantization errors on the observed velocities and that, due to the rounding operation, they are deterministically dependent upon  $\omega$  but, as explained in Sec. III, the uncertainty in the value of  $\omega$  translates into  $\zeta$  behaving as i.i.d. random variables with zero mean and uniform distribution.

If no statistical information about  $\bar{\mathbf{v}}$  is available, the least square estimator  $\hat{\bar{\mathbf{v}}} = (\bar{\mathbf{U}}\bar{\mathbf{U}}^\top)^{-1}\bar{\mathbf{U}}\bar{\boldsymbol{\omega}}$  could be exploited<sup>5</sup>. However, the above least square estimator cannot directly be applied for the following two reasons:

- The matrix  $\bar{\mathbf{U}}$  is a function of the unknown vectors  $\mathbf{p}_i$ ,  $i \in \mathcal{N}$ , for which only estimates are available. Then, in practice, we need to replace  $\bar{\mathbf{U}}$  in the above expression with the matrix  $\hat{\bar{\mathbf{U}}}$  computed using the estimated positions  $\hat{\mathbf{p}}_i$ ,  $i \in \mathcal{N}$ , obtained at the output of TIP.
- The observations  $\tilde{\omega}_{i,j,k}$  are only available as the elements  $v_{i,j,m}$  of the ordered lists  $\mathcal{V}_{i,j}$ . We recall that the relation between the terms  $\tilde{\omega}_{i,j,k}$  and  $v_{i,j,m}$  is completely defined by the maps  $\boldsymbol{\mu}$ , which are unknown. Hence, in a practical implementation, one must replace  $\tilde{\boldsymbol{\omega}}$  with  $\hat{\tilde{\boldsymbol{\omega}}}$ , obtained by reordering the lists  $\mathcal{V}$  using the estimated maps  $\hat{\boldsymbol{\mu}}$ .

It follows that the estimate of  $\bar{\mathbf{v}}$  can be obtained as

$$\hat{\bar{\mathbf{v}}} = \left( \hat{\bar{\mathbf{U}}}\hat{\bar{\mathbf{U}}}^\top \right)^{-1} \hat{\bar{\mathbf{U}}}\hat{\tilde{\boldsymbol{\omega}}}, \quad (29)$$

and it is affected by three sources of errors: the quantization error represented by the terms  $\zeta_{i,j,k}$ , the position error  $\mathbf{p} - \hat{\mathbf{p}}$ , and the error in estimating the maps  $\boldsymbol{\mu}$ .

## VI. TURBO ITERATIVE UAV POSITIONING AND TRACKING

The TIP algorithm schematized in Fig. 2 combines the methods presented in Sections III, IV, and V, in a high-performance iterative solution for estimating both positions and velocities of the UAVs. Here, we provide a detailed description of the TIP operational modes. In particular, first Sec. VI-A introduces the *cold start mode*, a version of TIP designed for the most challenging case where no prior knowledge about positions, velocities, or trajectories of the UAVs is available to the system. Then Sec. VI-B describes the *tracking mode* where UAVs follow a trajectory and provide channel profiles to the edge server once every  $\Delta t$  seconds. At each time step, TIP exploits the current channel profiles and the previous estimates of the positions and the velocities, to infer the current positions and velocities.

### A. Cold start mode

The pseudocode for TIP working in cold start mode is outlined in Algorithm 3. TIP takes as input the set of lists  $\mathcal{D}$  and  $\mathcal{V}$ , which are collected by the edge server. We recall that such lists contain the discretized delay-Doppler profiles of all channels connecting any pair of UAVs. As explained in Sec. II, the elements of list  $\mathcal{D}_{i,j}$  are the estimated path distances  $d_{i,j,m}$ ,  $m=1, \dots, N-1$ , ordered in increasing order. The first main challenge for estimating the UAV positions is

<sup>5</sup>When instead a prior distribution for  $\bar{\mathbf{v}}$  is known, better estimators (e.g., the maximum a posteriori estimator) can be used.

to associate each path distance  $d_{i,j,m}$  with the identity of the UAV that generated it, i.e., to find the maps  $\boldsymbol{\mu}$ . Such maps cannot be obtained deterministically, rather they have to be estimated. For this reason, the core of the TIP algorithm is a sophisticated mechanism designed for iteratively refining such maps. In the following, we denote by  $\hat{\boldsymbol{\mu}}^{(\ell)}$  the set of estimated maps at iteration  $\ell$ .

At iteration  $\ell=0$ , TIP first provides an initial estimate of the maps,  $\hat{\boldsymbol{\mu}}^{(0)}$ , directly from  $\mathcal{D}$  using the BP approach described in Algorithm 2. The estimated maps are then employed to reorder the lists  $\mathcal{D}$  and  $\mathcal{V}$  according to the rule specified in Sec. III-C. Specifically, at generic iteration  $\ell$ ,  $\hat{\boldsymbol{\mu}}_{i,j}^{(\ell)}$  is applied to  $\mathcal{D}_{i,j}$  and  $\mathcal{V}_{i,j}$  so as to reorder their elements according to the UAVs' identity index. In so doing, we obtain lists  $\hat{\Delta}_{i,j}^{(\ell)}$  and  $\hat{\Omega}_{i,j}^{(\ell)}$ , respectively, where their  $k$ -th elements,  $\hat{\delta}_{i,j,k}^{(\ell)}$  and  $\hat{\omega}_{i,j,k}^{(\ell)}$ , are an estimate of the distance  $\delta_{i,j,k}$  and of the velocity  $\omega_{i,j,k}$ , respectively. If the map is perfectly estimated, i.e.,  $\hat{\boldsymbol{\mu}}_{i,j}^{(\ell)} = \boldsymbol{\mu}_{i,j}$ , then  $\hat{\delta}_{i,j,k}^{(\ell)} = \delta_{i,j,k}$  and  $\hat{\omega}_{i,j,k}^{(\ell)} = \omega_{i,j,k}$ .

The set of reordered lists,  $\hat{\Delta}^{(\ell)} = \{\hat{\Delta}_{i,j}^{(\ell)} | i, j = 1 \dots, N, i \neq j\}$  is then fed to the GD algorithm described in Sec. IV. The GD algorithm is initialized with previous estimate  $\hat{\mathbf{p}}^{(\ell)}$ , if available; otherwise, it is initialized with a random vector  $\hat{\mathbf{p}}_{\text{cold start}}^{(0)}$ . The GD algorithm then outputs the estimated positions,  $\hat{\mathbf{p}}^{(\ell+1)}$ , which are employed to (i) provide an estimate of the velocities,  $\hat{\bar{\mathbf{v}}}^{(\ell+1)}$ , using the reordered set of lists  $\hat{\Omega}^{(\ell)} = \{\hat{\Omega}_{i,j}^{(\ell)} | i, j = 1 \dots, N, i \neq j\}$  and the procedure described in Sec. V and (ii) update the estimate of the maps.

This latter task, performed by the block labeled “Compute maps” in Fig. 2, follows the procedure outlined below:

- 1) from the estimated positions  $\hat{\mathbf{p}}^{(\ell)}$  and for each  $i \neq j$ , we compute the distances  $\delta_{i,j,k}^*$  using (3), as

$$\delta_{i,j,k}^* = |\hat{\mathbf{p}}_j^{(\ell)} - \hat{\mathbf{p}}_k^{(\ell)}| + |\hat{\mathbf{p}}_k^{(\ell)} - \hat{\mathbf{p}}_i^{(\ell)}| - |\hat{\mathbf{p}}_j^{(\ell)} - \hat{\mathbf{p}}_i^{(\ell)}|, \quad (30)$$

for  $k \in \{1, \dots, N\} \setminus \{i\}$ , and we arrange them in the list  $\Delta_{i,j}^*$ ;

- 2) the elements of  $\Delta_{i,j}^*$  are then ordered in ascending order to form the list  $\tilde{\Delta}_{i,j}^*$ ;
- 3) finally, the new estimated map  $\hat{\boldsymbol{\mu}}_{i,j}^{(\ell)}$  is defined as the rule that transforms  $\Delta_{i,j}^*$  into  $\tilde{\Delta}_{i,j}^*$ .

The new maps are then employed to provide a better reordering of the lists  $\mathcal{D}$  and  $\mathcal{V}$ . The algorithm proceeds iteratively until a desired number of iterations,  $L$ , has been performed.

### B. Tracking mode

We now consider the case where each UAV follows a trajectory in space that can be described by the position vectors  $\vec{P}_i(t)$  and velocity vectors  $\vec{V}_i(t) = \frac{d}{dt}\vec{P}_i(t)$ , which are functions of time  $t$ . While moving along the trajectory, UAVs periodically send to the edge server (say every  $\Delta t$  seconds) the channel profiles obtained through the OTFS channel estimation. Then, at time  $t$ , TIP takes as input the set of lists  $\mathcal{D}(t)$  and  $\mathcal{V}(t)$  and provides an estimate of the positions  $\hat{\mathbf{p}}(t)$  and velocities  $\hat{\bar{\mathbf{v}}}(t)$ . To ease this task, the algorithm also exploits an estimate of the UAVs positions previously obtained at time  $t - \Delta t$ .



---

**Algorithm 3** TIP algorithm: Cold start mode
 

---

**Require:**  $\mathcal{D}$ ,  $\mathcal{V}$ ,  $L$

**for**  $\ell \leftarrow 0$  to  $L - 1$  **do**

**if**  $\ell = 0$  **then**

$\hat{\boldsymbol{\mu}}^{(0)} \leftarrow \text{EstimateMaps}(\mathcal{D})$  (Algorithm 2)

$\hat{\mathbf{p}}^{(0)} \leftarrow \text{rand}$

**else**

**for**  $i, j = 1, \dots, N, j \neq i$  **do**

      Create the lists  $\Delta_{i,j}^*$  using  $\hat{\mathbf{p}}^{(\ell)}$  and (30)

      Sort each list  $\Delta_{i,j}^*$  in ascending order to obtain  $\tilde{\Delta}_{i,j}^*$

      Compute the map  $\hat{\mu}_{i,j}^{(\ell)}$  that yield  $\tilde{\Delta}_{i,j}^*$  from  $\Delta_{i,j}^*$

    Apply the maps  $\hat{\boldsymbol{\mu}}^{(\ell)}$  to  $\mathcal{D}$  to obtain  $\hat{\boldsymbol{\Delta}}^{(\ell)}$

    Apply the maps  $\hat{\boldsymbol{\mu}}^{(\ell)}$  to  $\mathcal{V}$  to obtain  $\hat{\boldsymbol{\Omega}}^{(\ell)}$

$\hat{\mathbf{p}}^{(\ell+1)} \leftarrow \text{GradientDescent}(\hat{\boldsymbol{\Delta}}^{(\ell)}, \hat{\mathbf{p}}^{(\ell)})$

    Compute  $\hat{\mathbf{v}}^{(\ell+1)}$  using (29)

$\ell \leftarrow \ell + 1$

**return**  $\hat{\mathbf{p}}^{(L)}$

---

In this scenario, TIP activates the tracking module depicted in Fig. 2. Also, since a prior estimate of the UAVs positions is already available, the cold start module starts from iteration  $\ell=1$  (instead of  $\ell=0$ ) and, consequently, the block named ‘‘Belief propagation’’ is not activated. The reason for this choice is that BP is able to infer reliable estimates of the maps when no prior information on the UAVs’ positions is available at a price of computational complexity  $O(N^8)$ . However, in tracking mode, the system has prior estimates of the UAVs’ positions, which makes the use of BP unnecessary. Apart from this aspect, the tracking module works as described in Sec. VI-A.

Summarizing, in tracking mode TIP works as follows. At time  $t$ , TIP

- gets as input the channel profiles  $\mathcal{D}(t)$  and  $\mathcal{V}(t)$ , as well as the prior estimate of the positions  $\mathbf{p}_{\text{tracking}}(t)$  obtained at time  $t - \Delta t$ ;
- provides a current estimate of the positions  $\hat{\mathbf{p}}(t)$  and of the velocities  $\hat{\mathbf{v}}(t)$ ;
- provides a forecast for the UAVs positions at time  $t + \Delta t$ , computed as

$$\mathbf{p}_{\text{tracking}}(t) = \hat{\mathbf{p}}(t) + \Delta t \hat{\mathbf{v}}(t).$$

### C. Genie aided TIP

To provide a benchmark for the performance of our proposed positioning algorithm, we consider a genie aided (GA) version of TIP which has perfect knowledge of the maps  $\boldsymbol{\mu}$ . The structure of the GA is a simplification of the scheme in Fig. 2 where  $L = 0$  (no iterations are performed) and the block ‘‘Apply maps’’ takes as input the actual maps, i.e.,  $\hat{\boldsymbol{\mu}}^{(0)} = \boldsymbol{\mu}$ . Consequently, in the GA version the blocks ‘‘Belief propagation’’ and ‘‘Apply maps’’ are unnecessary. As shown in Sec.VIII, GA will be used as a lower bound for the performance of TIP and as way to measure the ability of TIP to correctly estimate the maps.

## VII. CRAMÉR RAO LOWER BOUND ON JOINT POSITION-VELOCITY ESTIMATION

To provide a benchmark for the performance of the proposed TIP algorithm, we now derive the joint Cramér Rao lower bound (CRLB) to the variance of the UAVs’ position and velocity estimates. To this end, we assume that the set of maps  $\boldsymbol{\mu}$  is perfectly known, so that it is possible to correctly associate the elements of the lists  $\mathcal{D}_{i,j}$  and  $\mathcal{V}_{i,j}$  with the corresponding UAVs’ identities.

We recall that  $A$  UAV out of  $N$  are anchors, i.e., their positions and velocities are perfectly known. Therefore, the joint CRLB should only refer to the  $\bar{N}=N - A$  UAVs which are not anchors. Let  $\bar{\mathcal{N}}$  be the set of such UAVs and define  $\bar{\mathbf{p}}$  and  $\bar{\mathbf{v}}$  as the  $3\bar{N}$ -size vectors obtained by stacking the positions and velocities,  $\mathbf{p}_i$  and  $\mathbf{v}_i$ , respectively,  $\forall i \in \bar{\mathcal{N}}$ . In the CRLB terminology, the position and velocities  $\bar{\mathbf{p}}$  and  $\bar{\mathbf{v}}$  represent the parameters to be estimated, while the set of distance-velocities  $\mathcal{D}$  and  $\mathcal{V}$  are the observations. Hence, the total number of parameters to estimate is  $6\bar{N}$  i.e., 3 position components and 3 velocity components for each UAV in  $\bar{\mathcal{N}}$ .

Let us first consider the UAV’s positions and velocities vectors as random variables, whose components are i.i.d. and have density  $f_p(p)$  and  $f_v(v)$ , respectively. In other words, the joint density of the elements of  $\bar{\mathbf{p}}$  is  $f_{\bar{\mathbf{p}}}(\bar{\mathbf{p}}) = \prod_{\ell=1}^{3\bar{N}} f_p(\bar{p}_\ell)$  and, similarly,  $f_{\bar{\mathbf{v}}}(\bar{\mathbf{v}}) = \prod_{\ell=1}^{3\bar{N}} f_v(\bar{v}_\ell)$  where  $\bar{p}_\ell$  and  $\bar{v}_\ell$  are the  $\ell$ -th elements of  $\bar{\mathbf{p}}$  and  $\bar{\mathbf{v}}$ , respectively.

As already discussed in Sec. III, although the discretization errors  $\eta_{i,j,k}$  and  $\zeta_{i,j,k}$  appearing in (6) and (7) are functions of (hence, correlated with)  $\delta_{i,j,k}$  and  $v_{i,j,k}$  (resp.), the uncertainty in the UAVs’ positions and velocities can be translated into  $\eta_{i,j,k}$  and  $\zeta_{i,j,k}$  being i.i.d. random variables, with distributions  $f_\eta(\eta)$  and  $f_\zeta(\zeta)$  uniform in the ranges  $[-\frac{c}{2B}, \frac{c}{2B}]$  and  $[-\frac{c}{2f_c T_f}, \frac{c}{2f_c T_f}]$ , respectively. Such an assumption allows us to define the joint density of observations and parameters as  $f_{\mathcal{D}, \mathcal{V}, \bar{\mathbf{p}}, \bar{\mathbf{v}}}(\mathcal{D}, \mathcal{V}, \bar{\mathbf{p}}, \bar{\mathbf{v}})$ .

It follows that the joint CRLB on the  $\ell$ -th parameter to be estimated is given by  $[\mathbf{F}^{-1}]_{\ell,\ell}$  where  $\mathbf{F}$  is the  $6\bar{N} \times 6\bar{N}$  Fisher information matrix (FIM) defined as  $\mathbf{F} = \mathbb{E}_{\mathcal{D}, \mathcal{V}, \bar{\mathbf{p}}, \bar{\mathbf{v}}} [\mathbf{y}\mathbf{y}^T]$  where

$$\mathbf{y} = \begin{bmatrix} \frac{\partial}{\partial \bar{\mathbf{p}}} \log f_{\mathcal{D}, \mathcal{V}, \bar{\mathbf{p}}, \bar{\mathbf{v}}}(\mathcal{D}, \mathcal{V}, \bar{\mathbf{p}}, \bar{\mathbf{v}}) \\ \frac{\partial}{\partial \bar{\mathbf{v}}} \log f_{\mathcal{D}, \mathcal{V}, \bar{\mathbf{p}}, \bar{\mathbf{v}}}(\mathcal{D}, \mathcal{V}, \bar{\mathbf{p}}, \bar{\mathbf{v}}) \end{bmatrix} \quad (31)$$

The derivation of the expression of the FIM is quite tedious, and is summarized in Appendix B. The FIM is given by

$$\mathbf{F} = \begin{bmatrix} C_\eta \mathbf{D}_{p,p} + C_\zeta \mathbf{V}_{p,p} + C_p \mathbf{I} & C_\zeta \mathbf{V}_{p,v} \\ C_\zeta \mathbf{V}_{p,v}^T & C_\zeta \mathbf{V}_{v,v} + C_v \mathbf{I} \end{bmatrix}$$

where the matrices  $\mathbf{D}_{p,p}$ ,  $\mathbf{V}_{p,p}$ ,  $\mathbf{V}_{p,v}$ ,  $\mathbf{V}_{v,v}$  are defined in Appendix B and

$$C_x = \int_{\mathbb{R}} \frac{(f'_x(z))^2}{f_x(z)} dz, \quad (32)$$

$x \in \{p, v, \eta, \zeta\}$ . We point out that when  $f_x(x)$  is a uniform distributions, the coefficient  $C_x$  cannot be computed, due to the discontinuities in its expression. It follows that the joint CRLB cannot be computed under the hypothesis of uniformly distributed  $\eta_{i,j,k}$  and  $\zeta_{i,j,k}$ . To circumvent this problem, and only for the purpose of the CRLB evaluation, we assume

$\eta_{i,j,k} \sim \mathcal{N}(0, \sigma_\eta^2)$  and  $\zeta_{i,j,k} \sim \mathcal{N}(0, \sigma_\zeta^2)$  where  $\sigma_\eta = \frac{c^2}{\sqrt{12}B}$  and  $\sigma_\zeta = \frac{c}{\sqrt{12}f_c T_f}$  so that they have the same variance as their uniformly distributed counterparts. For a Gaussian distribution, the coefficient  $C_x$  is given by  $C_x = 1/\sigma_x^2$ .

The average joint *per-component* CRLB on the estimate of the position and velocity vectors are thus given by

$$\overline{\text{CRLB}}_p^{\text{joint}} = \frac{1}{3\bar{N}} \sum_{\ell=1}^{3\bar{N}} [\mathbf{F}^{-1}]_{\ell,\ell} \quad (33)$$

$$\overline{\text{CRLB}}_v^{\text{joint}} = \frac{1}{3\bar{N}} \sum_{\ell=3\bar{N}+1}^{6\bar{N}} [\mathbf{F}^{-1}]_{\ell,\ell}. \quad (34)$$

#### A. CRLB on the velocities, given the positions

In the TIP algorithm, estimates of the velocities are obtained from estimates of the positions, using a least squares estimator and following the procedure described in Sec. V. To benchmark the performance of the proposed velocity estimator, we derive the expression of the CRLB on the variance of  $\hat{\mathbf{v}}$ , given the actual UAV positions,  $\mathbf{p}$ .

We recall that the relation between the OTFS channel estimates,  $\tilde{\omega}$ , and the velocities,  $\mathbf{v}$ , is given by (28), where  $\mathbf{U}$  is a function of the actual positions  $\mathbf{p}$ . Assuming the elements of  $\zeta$  to be i.i.d. Gaussian with zero-mean and standard deviation  $\sigma_\zeta = \frac{c}{\sqrt{12}f_c T_f}$ , and the elements of  $\mathbf{v}$  i.i.d. Gaussian with zero-mean and variance  $\sigma_v^2$ , the joint distribution of  $\tilde{\omega}$  and  $\bar{\mathbf{v}}$  given  $\bar{\mathbf{U}}$  is proportional to

$$f_{\tilde{\omega}, \bar{\mathbf{v}} | \bar{\mathbf{U}}}(\tilde{\omega}) \propto e^{-\frac{1}{2\sigma_\zeta^2}(\tilde{\omega} - \bar{\mathbf{U}}\bar{\mathbf{v}})^\top(\tilde{\omega} - \bar{\mathbf{U}}\bar{\mathbf{v}})} e^{-\frac{1}{2\sigma_v^2}\bar{\mathbf{v}}^\top\bar{\mathbf{v}}}.$$

In this case, the FIM is given by

$$\mathbb{E}_{\tilde{\omega}, \bar{\mathbf{v}}} \left[ -\frac{\partial^2}{\partial \bar{\mathbf{v}} \partial \bar{\mathbf{v}}^\top} \log f_{\tilde{\omega}, \bar{\mathbf{v}} | \bar{\mathbf{U}}}(\tilde{\omega}) \right] = \frac{1}{\sigma_\zeta^2} \bar{\mathbf{U}}^\top \bar{\mathbf{U}} + \frac{1}{\sigma_v^2} \mathbf{I} \triangleq \mathbf{B}.$$

It follows that the CRLB on the estimate of the  $\ell$ -th element of  $\bar{\mathbf{v}}$  is given by  $\text{CRLB}_{v,\ell} = [\mathbf{B}^{-1}]_{\ell,\ell}$  and the average CRLB on the estimate of the velocity vectors  $\bar{\mathbf{V}}_i$  (per component) is

$$\overline{\text{CRLB}}_v = \frac{1}{3\bar{N}} \text{Tr} \{ \mathbf{B}^{-1} \}. \quad (35)$$

### VIII. NUMERICAL RESULTS

We now measure the performance of TIP by simulating some test scenarios. As performance metric, we consider the root mean square error (RMSE) on the position and velocity estimate per UAV and per dimension  $x, y, z$ . By recalling that  $\bar{\mathcal{N}}$  is the set of non-anchor UAVs, the RMSE on the position estimates is computed by averaging the results obtained from  $R$  runs of the TIP algorithm, as

$$\text{RMSE}_p = \sqrt{\frac{1}{3\bar{N}R} \sum_{i \in \bar{\mathcal{N}}} \sum_{r=1}^R |\hat{\mathbf{p}}_{i,r} - \mathbf{p}_{i,r}|^2} \quad (36)$$

where  $\mathbf{p}_{i,r}$  is the  $r$ -th realization of the positions  $\mathbf{p}_i$  and  $\hat{\mathbf{p}}_{i,r}$  is the corresponding estimate. Likewise, the RMSE on the velocity estimates is computed as

$$\text{RMSE}_v = \sqrt{\frac{1}{3\bar{N}R} \sum_{i \in \bar{\mathcal{N}}} \sum_{r=1}^R |\hat{\mathbf{v}}_{i,r} - \mathbf{v}_{i,r}|^2}. \quad (37)$$

As a test scenario, we consider a swarm composed of  $\bar{N}=4$  UAVs moving in a flight area and  $A=4$  anchors with fixed position (their velocity is zero). The  $N=\bar{N}+A$  UAVs plus anchors communicate among each other using signals with bandwidth  $B$  and central frequency  $f_c=5$  GHz. Specifically, we assume that anchors have identities  $i=1, 2, 3, 4$ , and their positions, measured in meters, are  $\bar{\mathbf{P}}_1=\mathbf{0}$ ,  $\bar{\mathbf{P}}_2=1000 \bar{\mathbf{e}}_x$ ,  $\bar{\mathbf{P}}_3=1000 \bar{\mathbf{e}}_y$ , and  $\bar{\mathbf{P}}_4=1000 \bar{\mathbf{e}}_z$ .

In the gradient descent algorithm, we set the stopping threshold to  $\epsilon=10^{-4}$  and the maximum number of iterations to  $I_\alpha = 100$ . For the gradient step  $\gamma$ , we employ the adaptive Barzilai-Borwein method [13], which ensures a faster convergence. Also, we set the threshold  $\bar{E}_b=2E_b$  in (25).

#### A. Cold start mode

We start by showing the performance of TIP in cold start mode. The results are obtained by averaging the output of TIP over  $R=100$  runs. At each run, the components of the UAV's position vectors were randomly drawn from  $\mathcal{N}(\mu, \sigma^2)$  with  $\mu=500$  m and  $\sigma=\frac{1,000}{\sqrt{12}} \approx 289$  m.<sup>6</sup> Also, at each run, TIP is initialized by drawing each component of the tentative positions  $\hat{\mathbf{p}}_{\text{cold start}}^{(0)}$  from the same Gaussian distribution. Likewise, at each run, the components of the UAVs velocity vectors were randomly drawn from  $\mathcal{N}(0, \sigma^2)$  with  $\sigma=10$  m/s.

Fig. 3(left) shows the  $\text{RMSE}_p$  in (36) achieved by TIP, plotted versus the number of iterations of the gradient descent algorithm,  $I_\alpha$ , for  $L=0$  (no TIP iterations) and signal bandwidth  $B=15$  MHz, corresponding to a discretization step  $c/B=20$  m. One can notice that  $I_\mu=5$  iterations of the BP algorithm provide the same performance as the genie-aided (GA) algorithm, which has perfect knowledge of the maps  $\boldsymbol{\mu}$ . We recall that GA is used here as benchmark since it represents a lower bound for the TIP  $\text{RMSE}_p$ . Fig. 3(left) underlines that, despite 20 m discretization step in the measurements, the system achieves an  $\text{RMSE}_p$  of about 1 m after  $I_\alpha=50$  iterations, which means that BP provides very reliable estimates  $\hat{\boldsymbol{\mu}}$ . However, for a smaller bandwidth,  $B=3$  MHz, such

<sup>6</sup>These are the same  $\mu$  and  $\sigma$  of a uniform distribution of UAVs in a cube of side 1,000 m with vertices coinciding with the four anchor nodes.

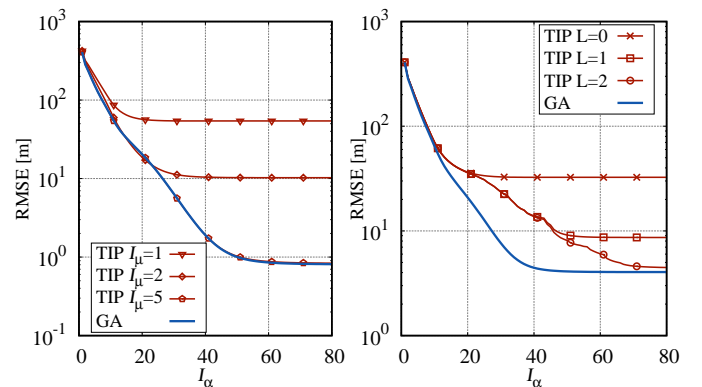


Fig. 3. RMSE as a function of the number of gradient descent iterations ( $I_\alpha$ ). Left:  $L=0$  and  $B=15$  MHz corresponding to  $c\Delta\tau=20$  m. Right:  $I_\mu=5$  and  $B=3$  MHz corresponding to  $c\Delta\tau=100$  m.

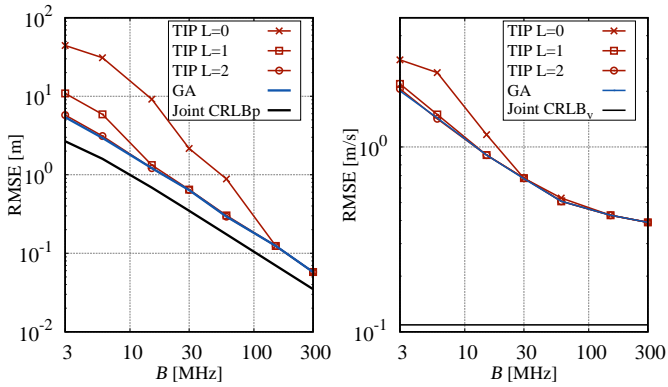


Fig. 4. RMSE on position estimates (left) and velocity estimates (right), as a function of the signal bandwidth, for varying  $L$ , and  $I_\mu=2$ . Average over random UAV positions.

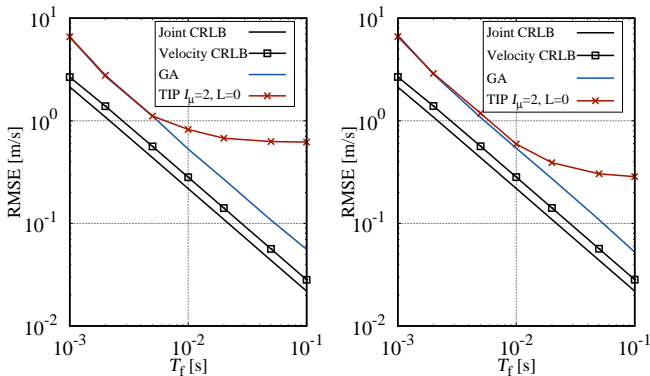


Fig. 5. RMSE on velocity estimation as a function of the frame time, for  $B = 30$  MHz (left) and  $B = 300$  MHz (right).

estimates have much lower reliability: some TIP iterations are then required to improve the  $\text{RMSE}_p$ , as in the example shown in Fig. 3(right). Here the discretization step is  $c/B=100$  m and the number of BP iterations is  $I_\mu=5$ . For  $L=0$  (no TIP iterations), the resulting  $\text{RMSE}_p$  is quite large, about 50 m, while a single TIP iteration lowers it at about 10 m. Importantly, with a further TIP iteration ( $L=2$ ) and  $I_\alpha > 70$  iterations, the system reaches the GA performance.

Fig. 4(left) presents the  $\text{RMSE}_p$  in (36) versus the signal bandwidth,  $B$ , as the number of TIP iterations,  $L$ , varies, for  $I_\mu=2$ . For the sake of comparison, the figure also shows the performance of the GA algorithm, and the joint CRLB computed according to (33). We observe that, as  $B$  increases, the discretization step decreases and the system provides, in general, more accurate positioning. For  $L=2$ , the system performance reaches the GA for all considered values of  $B$  in the range 3–300 MHz. Interestingly, the GA is very close to the CRLB leaving negligible room for improvements for other positioning techniques. For the same system parameters and for frame time  $T_f=20$  ms, Fig. 4(right) shows the  $\text{RMSE}_v$  in (37) on the estimate of the UAV velocities, measured in m/s, plotted versus the signal bandwidth. For such a value of  $T_f$ , the discretization step on the velocities is  $c/f_c T_f=3$  m/s. As can be observed,  $L=2$  iterations are enough for TIP to achieve the performance of GA, and for  $B=300$  MHz the achieved  $\text{RMSE}_v \approx 0.4$  m/s, which is well below the discretization step.

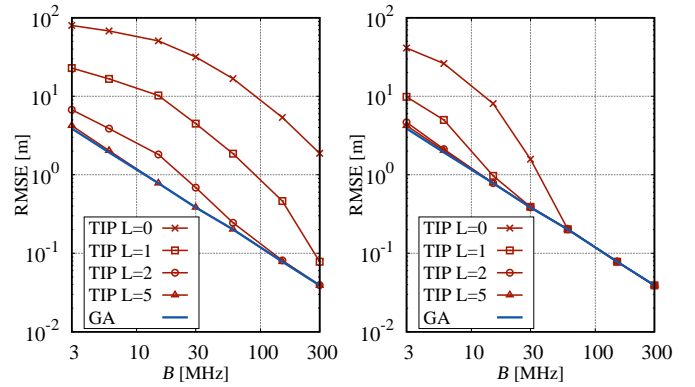


Fig. 6. RMSE on position estimation as a function of the signal bandwidth as  $L$  varies, for  $I_\mu=1$  (left) and  $I_\mu=2$  (right). Average over UAV positions along real-world trajectories from [14].

Fig. 5 illustrates the performance of the GA algorithm, the joint CRLB computed as in (34), and the CRLB on the velocities computed according to (35). The figure shows that the TIP algorithm performs very close to the GA for small to medium  $T_f$ . As  $T_f$  grows, quantization errors on the velocities reduce, while those on the distances (which depend on  $B$ ) become prominent. This explains why TIP performance shows a floor at about 0.7 m/s for  $B=30$  MHz, and about 0.25 m/s for  $B=300$  MHz.

The gap between GA and TIP for large  $T_f$  and large  $B$  can be explained as follows: when  $B$  is large and TIP converges, the maps  $\mu$  are estimated with high reliability. We recall that, if  $\mu_{i,j}(m)=k$ , then the  $m$ -th element of the map  $\mu_{i,j}$  associates the distance  $d_{i,j,m}$  of the ordered list  $\mathcal{D}_{i,j}$  with the identity of the  $k$ -th UAV. However, if an error occurs in estimating the map,  $\hat{\mu}_{i,j}$  associates with  $k$  the distance  $d_{i,j,m'}$ , instead of  $d_{i,j,m}$ . Nevertheless, if the map is highly reliable, we expect  $d_{i,j,m'}$  and  $d_{i,j,m}$  to have approximately the same value so that the degradation in terms of  $\text{RMSE}_p$  is negligible. The same estimated map, however, is also applied to lists  $\mathcal{V}_{i,j}$  and associates with  $k$  the velocity  $v_{i,j,m'}$  instead of  $v_{i,j,m}$ . The values of these two elements of  $\mathcal{V}_{i,j}$  may differ significantly so that, by exchanging them, we incur in a severe performance degradation. The GA scheme, on the other hand, having perfect knowledge of the maps does not suffer from this problem and its performance approaches the CRLB.

Fig. 6 presents the RMSE on the position estimates, computed by averaging over the set of real UAV positions available in [14], whose coordinates have been linearly scaled so as to fit in a cube of side 1,000 m centered at  $[500, 500, 500]$  m. All other parameters are the same as in Fig. 4. All curves are very similar to the ones shown in Fig. 4 even though the UAV locations are not random. This demonstrates that our theoretical analysis does apply to real-world scenarios.

## B. Tracking mode

To assess the performance of TIP in tracking mode, we consider a test scenario where the UAVs follow trajectories that are deterministic functions of time. As an example of

such trajectories, we choose the 3D Lissajous curve [15] which exhibits a simple and easy-to-implement parametric expression. The position vector of UAV  $i$  following a Lissajous trajectory  $\vec{P}_i(t) = p_{i,x}(t)\vec{e}_x + p_{i,y}(t)\vec{e}_y + p_{i,z}(t)\vec{e}_z$  whose components are given by:  $p_{i,s}(t) = a_{i,s} \sin(b_{i,s}t + \phi_{i,s})$  where  $a_{i,s}$ ,  $b_{i,s}$ , and  $\phi_{i,s}$  are parameters and  $s \in \{x, y, z\}$ . As a consequence, the instantaneous velocity vector of the  $i$ -th UAV is given by  $\vec{V}_i(t) = v_{i,x}(t)\vec{e}_x + v_{i,y}(t)\vec{e}_y + v_{i,z}(t)\vec{e}_z$  with components

$$v_{i,s}(t) = \frac{dp_{i,s}(t)}{dt} = a_{i,s}b_{i,s} \cos(b_{i,s}t + \phi_{i,s}) \quad (38)$$

for  $s \in \{x, y, z\}$ .

Fig. 7 depicts a 2D projection of a portion of the same 3D Lissajous trajectory. This is an instance of a random trajectory obtained by independently drawing the parameters  $a_{i,s}$  from the uniform distribution  $\mathcal{U}[0, 1]$ ,  $b_{i,s}$  from  $\mathcal{U}[0, 0.2]$ , and  $\phi_{i,\ell}$  from  $\mathcal{U}[0, 2\pi]$ . The signal bandwidth is set to  $B=10$  MHz and  $B=300$  MHz, in Fig. 7(left) and Fig. 7(right), respectively. In both figures,  $T_f=20$  ms, and the update time is  $\Delta t=1$  s. In the plots, the UAV trajectory is represented by the solid black line, while blue circles refer to the UAV position,  $\vec{P}_i(t)$  at  $t=n\Delta t$ ,  $n=0, 1, \dots, 50$ . The red circles denote the positions  $\hat{\vec{P}}_i(n\Delta t)$  estimated by TIP for  $L=5$  and the arrows represent the estimated velocity vectors  $\hat{\vec{V}}_i(n\Delta t)$ . The actual velocity vectors  $\vec{V}_i(n\Delta t)$  (not shown) are tangent to the black line at  $t=n\Delta t$ . The trajectory is travelled by the UAV from right to left and the blue circles mark 1 s-time intervals. For  $B=10$  MHz, the positions are well estimated (i.e., the red circles are always very close to the blue ones). However, errors in estimating the maps sometimes result in a poor estimate of the velocity vectors, in both direction and magnitude. By increasing the bandwidth to 300 MHz, the maps estimates become much more reliable: position estimates are excellent and the velocity vectors perfectly follow the tangent to the trajectory.

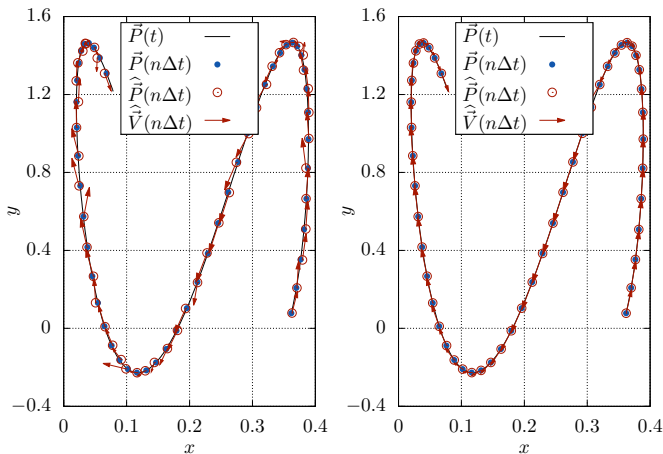


Fig. 7. 2D projection of a portion of a UAV Lissajous trajectory, for  $N=8$ ,  $A=4$ ,  $B=10$  MHz (left) and  $B=300$  MHz (right),  $T_f=20$  ms, and  $\Delta t=1$  s. The solid black line represents the trajectory, while blue circles indicate the UAV positions,  $\vec{P}_i(n\Delta t)$ . The red circles denote  $\hat{\vec{P}}_i(n\Delta t)$ . The arrows represent the estimated velocity vectors  $\hat{\vec{V}}_i(t)$ .

## IX. CONCLUSIONS

We proposed an iterative algorithm, named TIP, for localizing and tracking the position of UAVs communicating with each other, by using TDoA measurements obtained through OTFS-modulated signals. TIP exploits belief propagation and gradient descent optimization, to achieve precise positions and velocities of the UAVs even in the presence of limited OTFS channel estimation accuracy due to the limited resolution of the delay and Doppler shift grid. Taking advantage of the measurements from all the communications links between the UAVs, the remarkable advantage of our solution is that it increases by a factor 6-7 the localization accuracy over a multi-target radar system with a limited bandwidth  $B$ , which has a resolution of  $c/B$ . As no other algorithm using delay-Doppler channel measurements is available in the literature, we showed the excellent performance of TIP against the Cramér Rao lower bound and a genie aided version of TIP (with perfect knowledge of the maps). Future work will extend our method to include passive reflectors for terrestrial applications.

### APPENDIX A

#### DERIVATION OF (4)

Let  $\vec{P}_i$  be the position vector of UAV  $i$  at time  $t=0$  and  $\vec{V}_i$  its instantaneous velocity vector. Then, for small  $t$ , the position of  $i$  can be written as  $\vec{P}_i(t) = \vec{P}_i + t\vec{V}_i + o(t^2)$  or, in terms of their components,  $\mathbf{p}_i(t) = \mathbf{p}_i + t\mathbf{v}_i + o(t^2)$ .

The velocity of UAV  $j$  as observed by  $i$  through the reflexion on  $k$  is the derivative w.r.t. time (evaluated at  $t=0$ ) of the distance  $s_{i,j,k}(t)$  between  $j$  and  $i$  through  $k$ . In turn, this distance is the sum of two contributions: the distance between  $j$  and  $k$ , and the distance between  $k$  and  $i$ . Hence,

$$s_{i,j,k}(t) = |\mathbf{p}_j(t) - \mathbf{p}_k(t)| + |\mathbf{p}_k(t) - \mathbf{p}_i(t)|.$$

By using the chain rule, for any  $n$  and  $m$ , we get

$$\left. \frac{d|\mathbf{p}_n(t) - \mathbf{p}_m(t)|}{dt} \right|_{t=0} = (\mathbf{v}_n - \mathbf{v}_m)^\top \frac{\mathbf{p}_n - \mathbf{p}_m}{|\mathbf{p}_n - \mathbf{p}_m|}. \quad (39)$$

It follows that the expression for  $\omega_{i,j,k}$  is given by (4).

### APPENDIX B

#### CRAMER RAO LOWER BOUND

In the following, we summarize the procedure to derive the FIM  $\mathbf{F}$ . By conditioning over  $\bar{\mathbf{p}}$  and  $\bar{\mathbf{v}}$ , we can rewrite the joint density as

$$f_{\mathcal{D}, \mathcal{V}, \bar{\mathbf{p}}, \bar{\mathbf{v}}}(\mathcal{D}, \mathcal{V}, \bar{\mathbf{p}}, \bar{\mathbf{v}}) = f_{\mathcal{D}, \mathcal{V} | \bar{\mathbf{p}}, \bar{\mathbf{v}}}(\mathcal{D}, \mathcal{V} | \bar{\mathbf{p}}, \bar{\mathbf{v}}) f_{\bar{\mathbf{p}}}(\bar{\mathbf{p}}) f_{\bar{\mathbf{v}}}(\bar{\mathbf{v}}).$$

Then, by assuming that the OTFS delay and Doppler estimates are corrupted by independent quantization errors, we can write

$$\begin{aligned} f_{\mathcal{D}, \mathcal{V} | \bar{\mathbf{p}}, \bar{\mathbf{v}}}(\mathcal{D}, \mathcal{V} | \bar{\mathbf{p}}, \bar{\mathbf{v}}) &= f_{\mathcal{D} | \bar{\mathbf{p}}, \bar{\mathbf{v}}}(\mathcal{D} | \bar{\mathbf{p}}, \bar{\mathbf{v}}) f_{\mathcal{V} | \bar{\mathbf{p}}, \bar{\mathbf{v}}}(\mathcal{V} | \bar{\mathbf{p}}, \bar{\mathbf{v}}) \quad (40) \\ &\stackrel{(a)}{=} f_{\mathcal{D} | \bar{\mathbf{p}}}(\mathcal{D} | \bar{\mathbf{p}}) f_{\mathcal{V} | \bar{\mathbf{p}}, \bar{\mathbf{v}}}(\mathcal{V} | \bar{\mathbf{p}}, \bar{\mathbf{v}}) \\ &\stackrel{(b)}{=} \prod_{\substack{i,j \neq i, \\ k \neq \{i,j\}}} f_{\tilde{\delta}_{i,j,k} | \bar{\mathbf{p}}}(\tilde{\delta}_{i,j,k} | \bar{\mathbf{p}}) \times \prod_{\substack{i,j \neq i, \\ k \neq i}} f_{\tilde{v}_{i,j,k} | \bar{\mathbf{p}}, \bar{\mathbf{v}}}(\tilde{v}_{i,j,k} | \bar{\mathbf{p}}, \bar{\mathbf{v}}) \\ &\stackrel{(c)}{=} \prod_{\substack{i,j \neq i, \\ k \neq \{i,j\}}} f_{\eta_{i,j,k}}(\tilde{\delta}_{i,j,k} - \delta_{i,j,k}) \times \prod_{\substack{i,j \neq i, \\ k \neq i}} f_{\zeta_{i,j,k}}(\tilde{v}_{i,j,k} - v_{i,j,k}) \end{aligned}$$

In the equality (a), we exploited the fact that distances do not depend upon velocities, as granted by (3); in the equality (b) we exploited the independence among the elements of the lists in  $\mathcal{D}$  and  $\mathcal{V}$ , and the perfect knowledge of the maps  $\boldsymbol{\mu}$ . Finally, in (c) we used (6) and (7). Given the above results, we can rewrite (31) as

$$\mathbf{y} = \begin{bmatrix} \mathbf{c}_p + \mathbf{w}_p + \boldsymbol{\gamma}_p \\ \mathbf{w}_v + \boldsymbol{\gamma}_v \end{bmatrix} \quad \text{where}$$

$$\mathbf{c}_p \triangleq - \sum_{\substack{i,j \neq i, \\ k \neq \{i,j\}}} \left( \frac{\partial \delta_{i,j,k}}{\partial \bar{\mathbf{p}}} \right) \frac{f'_{\eta_{i,j,k}}(\tilde{\delta}_{i,j,k} - \delta_{i,j,k})}{f_{\eta_{i,j,k}}(\tilde{\delta}_{i,j,k} - \delta_{i,j,k})}, \quad (41)$$

$$\mathbf{w}_p \triangleq - \sum_{\substack{i,j \neq i, \\ k \neq i}} \left( \frac{\partial v_{i,j,k}}{\partial \bar{\mathbf{p}}} \right) \frac{f'_{\zeta_{i,j,k}}(\tilde{v}_{i,j,k} - v_{i,j,k})}{f_{\zeta_{i,j,k}}(\tilde{v}_{i,j,k} - v_{i,j,k})}, \quad (42)$$

$$\mathbf{w}_v \triangleq - \sum_{\substack{i,j \neq i, \\ k \neq i}} \left( \frac{\partial v_{i,j,k}}{\partial \bar{\mathbf{v}}} \right) \frac{f'_{\zeta_{i,j,k}}(\tilde{v}_{i,j,k} - v_{i,j,k})}{f_{\zeta_{i,j,k}}(\tilde{v}_{i,j,k} - v_{i,j,k})}, \quad (43)$$

$$\boldsymbol{\gamma}_p \triangleq \frac{\partial}{\partial \bar{\mathbf{p}}} \log f_{\bar{\mathbf{p}}}(\bar{\mathbf{p}}), \quad \boldsymbol{\gamma}_v \triangleq \frac{\partial}{\partial \bar{\mathbf{v}}} \log f_{\bar{\mathbf{v}}}(\bar{\mathbf{v}}). \quad (44)$$

For notation simplicity, let us define  $\mathbb{E}[\cdot] \triangleq \mathbb{E}_{\mathcal{D}, \mathcal{V}, \bar{\mathbf{p}}, \bar{\mathbf{v}}}[\cdot]$  as the average over all random variables. Then the FIM is given by

$$\mathbf{F} = \mathbb{E} \begin{bmatrix} \mathbf{h}\mathbf{h}^\top & \mathbf{h}(\mathbf{w}_v + \boldsymbol{\gamma}_v)^\top \\ (\mathbf{w}_v + \boldsymbol{\gamma}_v)\mathbf{h}^\top & (\mathbf{w}_v + \boldsymbol{\gamma}_v)(\mathbf{w}_v + \boldsymbol{\gamma}_v)^\top \end{bmatrix} \quad (45)$$

where  $\mathbf{h} \triangleq \mathbf{c}_p + \mathbf{w}_p + \boldsymbol{\gamma}_p$ . Note that most of the terms in (45) vanish. For example,  $\mathbb{E}[\mathbf{c}_p \boldsymbol{\gamma}_p^\top] = \mathbb{E}_{\mathcal{D}, \bar{\mathbf{p}}}[\mathbf{c}_p \boldsymbol{\gamma}_p^\top] = \mathbb{E}_{\bar{\mathbf{p}}}[\mathbb{E}_{\mathcal{D}|\bar{\mathbf{p}}}[\mathbf{c}_p] \boldsymbol{\gamma}_p^\top]$  since both  $\mathbf{c}_p$  and  $\boldsymbol{\gamma}_p$  do not depend upon  $\mathcal{V}$  and  $\bar{\mathbf{v}}$ . Also, by applying the definition of  $\mathbf{c}_p$  in (41),

$$\mathbb{E}_{\mathcal{D}|\bar{\mathbf{p}}}[\mathbf{c}_p] = - \sum_{\substack{i,j \neq i, \\ k \neq \{i,j\}}} \left( \frac{\partial \delta_{i,j,k}}{\partial \bar{\mathbf{p}}} \right) \mathbb{E}_{\mathcal{D}|\bar{\mathbf{p}}} \left[ \frac{f'_{\eta_{i,j,k}}(\tilde{\delta}_{i,j,k} - \delta_{i,j,k})}{f_{\eta_{i,j,k}}(\tilde{\delta}_{i,j,k} - \delta_{i,j,k})} \right] \quad (46)$$

Finally,

$$\begin{aligned} \mathbb{E}_{\mathcal{D}|\bar{\mathbf{p}}} \left[ \frac{f'_{\eta_{i,j,k}}(\tilde{\delta}_{i,j,k} - \delta_{i,j,k})}{f_{\eta_{i,j,k}}(\tilde{\delta}_{i,j,k} - \delta_{i,j,k})} \right] &= \int_{\mathbb{R}} f'_{\eta_{i,j,k}}(\tilde{\delta}_{i,j,k} - \delta_{i,j,k}) d\tilde{\delta}_{i,j,k} \\ &= f_{\eta_{i,j,k}}(\tilde{\delta}_{i,j,k} - \delta_{i,j,k}) \Big|_{-\infty}^{+\infty} = 0 \end{aligned} \quad (47)$$

By using the same procedure, it is easy to show that  $\mathbb{E}[\mathbf{w}_p \boldsymbol{\gamma}_p^\top] = \mathbf{0}$ ,  $\mathbb{E}[\mathbf{c}_p \mathbf{w}_p^\top] = \mathbf{0}$ ,  $\mathbb{E}[\mathbf{c}_p \mathbf{w}_v^\top] = \mathbf{0}$ ,  $\mathbb{E}[\mathbf{c}_p \boldsymbol{\gamma}_v^\top] = \mathbf{0}$ ,  $\mathbb{E}[\mathbf{w}_p \boldsymbol{\gamma}_v^\top] = \mathbf{0}$ ,  $\mathbb{E}[\mathbf{w}_v \boldsymbol{\gamma}_v^\top] = \mathbf{0}$ , and  $\mathbb{E}[\boldsymbol{\gamma}_p \boldsymbol{\gamma}_v^\top] = \mathbf{0}$ . Also  $\mathbb{E}[\boldsymbol{\gamma}_p \boldsymbol{\gamma}_p^\top] = C_p \mathbf{I}$  and  $\mathbb{E}[\boldsymbol{\gamma}_v \boldsymbol{\gamma}_v^\top] = C_v \mathbf{I}$  where the coefficients  $C_x$  are defined in (32). Hence, the FIM reduces to

$$\mathbf{F} = \begin{bmatrix} C_\eta \mathbf{D}_{p,p} + C_\zeta \mathbf{V}_{p,p} + C_p \mathbf{I} & C_\zeta \mathbf{V}_{p,v} \\ C_\zeta \mathbf{V}_{p,v}^\top & C_\zeta \mathbf{V}_{v,v} + C_v \mathbf{I} \end{bmatrix}$$

where  $C_x = \int_{\mathbb{R}} \frac{(f'_x(x))^2}{f_x(x)} dx$ ,  $x \in \{p, v, \eta, \zeta\}$  and

$$\mathbf{D}_{p,p} = \sum_{i,j \neq i, k \neq \{i,j\}} \mathbb{E}_{\bar{\mathbf{p}}} \left[ \frac{\partial \delta_{i,j,k}}{\partial \bar{\mathbf{p}}} \frac{\partial \delta_{i,j,k}}{\partial \bar{\mathbf{p}}^\top} \right],$$

$$\begin{aligned} \mathbf{V}_{p,p} &= \sum_{i,j \neq i, k \neq i} \mathbb{E}_{\bar{\mathbf{p}}, \bar{\mathbf{v}}} \left[ \frac{\partial v_{i,j,k}}{\partial \bar{\mathbf{p}}} \frac{\partial v_{i,j,k}}{\partial \bar{\mathbf{p}}^\top} \right], \\ \mathbf{V}_{p,v} &= \sum_{i,j \neq i, k \neq i} \mathbb{E}_{\bar{\mathbf{p}}, \bar{\mathbf{v}}} \left[ \frac{\partial v_{i,j,k}}{\partial \bar{\mathbf{p}}} \frac{\partial v_{i,j,k}}{\partial \bar{\mathbf{v}}^\top} \right], \\ \mathbf{V}_{v,v} &= \sum_{i,j \neq i, k \neq i} \mathbb{E}_{\bar{\mathbf{p}}, \bar{\mathbf{v}}} \left[ \frac{\partial v_{i,j,k}}{\partial \bar{\mathbf{v}}} \frac{\partial v_{i,j,k}}{\partial \bar{\mathbf{v}}^\top} \right]. \end{aligned} \quad (48)$$

By defining  $\mathbf{q}_{m,n} \triangleq \frac{\mathbf{v}_m - \mathbf{v}_n}{\|\mathbf{p}_m - \mathbf{p}_n\|}$  and by recalling (3) and (4), for any  $h \in \bar{\mathcal{N}}$

$$\frac{\partial \delta_{i,j,k}}{\partial \mathbf{p}_h} = \begin{cases} \mathbf{u}_{i,k} - \mathbf{u}_{i,j}, & h=i \\ \mathbf{u}_{j,k} - \mathbf{u}_{j,i}, & h=j \\ \mathbf{u}_{k,i} + \mathbf{u}_{k,j}, & h=k \\ \mathbf{0} & \text{otherwise} \end{cases} \quad \frac{\partial v_{i,j,k}}{\partial \mathbf{v}_h} = \begin{cases} \mathbf{u}_{i,k}, & h=i \\ -\mathbf{u}_{k,j}, & h=j \\ -\mathbf{u}_{i,k} + \mathbf{u}_{k,j}, & h=k \\ \mathbf{0} & \text{otherwise} \end{cases}$$

$$\frac{\partial v_{i,j,k}}{\partial \mathbf{p}_h} = \begin{cases} \mathbf{q}_{i,k} - (\mathbf{q}_{i,k}^\top \mathbf{u}_{i,k}) \mathbf{u}_{i,k} & \text{if } h=i \\ -\mathbf{q}_{k,j} + (\mathbf{q}_{k,j}^\top \mathbf{u}_{k,j}) \mathbf{u}_{k,j} & \text{if } h=j \\ \mathbf{q}_{k,j} - \mathbf{q}_{i,k} + (\mathbf{q}_{i,k}^\top \mathbf{u}_{i,k}) \mathbf{u}_{i,k} & \text{if } h=k \\ \mathbf{0} & \text{else.} \end{cases}$$

## REFERENCES

- [1] A. Nordio, C. F. Chiasserini, and E. Viterbo, "Robust Localization of UAVs in OTFS-Based Networks," in *2023 IEEE Global Communications Conference (GLOBECOM)*, 12 2023, accepted for presentation.
- [2] K. Witrals, P. Meissner, E. Leitinger, Y. Shen, C. Gustafson, F. Tufvesson, K. Haneda, D. Dardari, A. F. Molisch, A. Conti, and M. Z. Win, "High-accuracy localization for assisted living: 5G systems will turn multipath channels from foe to friend," *IEEE Signal Processing Magazine*, vol. 33, no. 2, pp. 59–70, 2016.
- [3] A. R. Ansari, N. Saeed, M. I. Ul Haq, and S. Cho, "Accurate 3D localization method for public safety applications in vehicular ad-hoc networks," *IEEE Access*, vol. 6, pp. 20 756–20 763, 2018.
- [4] S. M. Asaad and H. S. Maghddid, "A comprehensive review of indoor/outdoor localization solutions in IoT era: Research challenges and future perspectives," *Computer Networks*, vol. 212, p. 109041, 2022.
- [5] L. Han, R. Liu, X. Lv, Z. Wang, and Q. Zhu, "Optimal waveform design for integrated localization and communication in OFDM systems," in *2022 IEEE 8th International Conference on Computer and Communications (ICCC)*, 2022, pp. 868–874.
- [6] J. Bai, G. Wei, S. Wang, X. Wang, and Z. Fei, "Efficient direct localization of OFDM emitters in multipath environment with mobile receivers," *IEEE Transactions on Vehicular Technology*, vol. 71, no. 1, pp. 545–556, 2022.
- [7] M. J. Emadi, S. Hu, and H. Wang, "Precise positioning: When OTFS meets distributed cooperative positioning," Feb. 2023. [Online]. Available: 10.36227/techrxiv.21951014.v1
- [8] F. Linsalata, A. Albanese, V. Sciancalepore, F. Roveda, M. Magarini, and X. Costa-Perez, "OTFS-superimposed PRACH-aided localization for UAV safety applications," in *2021 IEEE Global Communications Conference (GLOBECOM)*, 2021, pp. 1–6.
- [9] Y. Hong, T. Thaj, and E. Viterbo, *Delay-Doppler Communications: Principles and Applications*. Academic Press, Elsevier, 2022.
- [10] L. Wielandner, E. Leitinger, F. Meyer, and K. Witrals, "Message passing-based 9-D cooperative localization and navigation with embedded particle flow," *IEEE Transactions on Signal and Information Processing over Networks*, vol. 9, pp. 95–109, 2023.
- [11] E. Leitinger, F. Meyer, F. Hlawatsch, K. Witrals, F. Tufvesson, and M. Z. Win, "A belief propagation algorithm for multipath-based SLAM," *IEEE Transactions on Wireless Communications*, vol. 18, no. 12, pp. 5613–5629, 2019.
- [12] P. Raviteja, K. T. Phan, and Y. Hong, "Embedded Pilot-Aided Channel Estimation for OTFS in Delay-Doppler Channels," *IEEE Trans. Veh. Tech.*, vol. 68, no. 5, pp. 4906–4917, 2019.
- [13] J. Barzilay and J. M. Borwein, "Two-Point Step Size Gradient Methods," *IMA Journal of Numerical Analysis*, vol. 8, no. 1, pp. 141–148, 01 1988. [Online]. Available: <https://doi.org/10.1093/imanum/8.1.141>
- [14] "Drone tracking dataset," <https://github.com/CenekAlbl/drone-tracking-datasets>.
- [15] M. G. V. Bogle, J. E. Hearst, V. F. R. Jones, and L. Stoilov, "Lissajous knots," *Journal of Knot Theory and Its Ramifications*, vol. 03, no. 02, pp. 121–140, 1994.